

Classification of Subpulse Drifting in Pulsars

Rahul Basu¹, Dipanjan Mitra^{2,3}, George I. Melikidze^{3,4}, Anna Skrzypczak³

¹ *Inter-University Centre for Astronomy and Astrophysics, Pune, 411007, India; rahulbasu.astro@gmail.com*

² *National Centre for Radio Astrophysics, Tata Institute of Fundamental Research, Pune 411007, India*

³ *Janusz Gil Institute of Astronomy, University of Zielona Góra, ul. Szafrana 2, 65-516 Zielona Góra, Poland*

⁴ *Abastumani Astrophysical Observatory, Iliia State University, 3-5 Cholokashvili Ave., Tbilisi, 0160, Georgia*

9 August 2021

ABSTRACT

In this study we propose a classification scheme for the phenomenon of subpulse drifting in pulsars. We have assembled an exhaustive list of pulsars which exhibit subpulse drifting from previously published results as well as recent observations using the Giant Meterwave Radio Telescope. We have estimated detailed phase variations corresponding to the drifting features. Based on phase behaviour the drifting population was classified into four groups : coherent phase-modulated drifting, switching phase-modulated drifting, diffuse phase-modulated drifting and low-mixed phase-modulated drifting. We have re-established the previous assertion that the subpulse drifting is primarily associated with the conal components in pulsar profile. The core components generally do not show the drifting phenomenon. However, in core emission of certain pulsars longer periodic fluctuations are seen, which are similar to periodic nulling, and likely arise due to a different physical phenomenon. In general the nature of the phase variations of the drifting features across the pulsar profile appears to be associated with specific pulsar profile classes, but we also find several examples that show departures from this trend. It has also been claimed in previous works that the spin-down energy loss is anti-correlated with the drifting periodicity. We have verified this dependence using a larger sample of drifting measurements.

Key words: pulsars: general

1 INTRODUCTION

The single pulse emission from pulsars consist of one or more components which are known as subpulses. Shortly after the discovery of pulsars it was observed that the subpulses in some cases carry out systematic drift motion within the pulse window and the phenomenon was termed subpulse drifting (Drake & Craft 1968). A systematic approach to measuring drifting features was developed by Backer (1973); Backer *et al.* (1975), which included the fluctuation spectral studies. The drifting is usually characterised by two periodicities, P_2 , the longitudinal separation between two adjacent drift bands, and P_3 , the interval over which the subpulses repeat at any specific location within the pulse window. Fluctuation spectral studies estimate the Fourier transform of the subpulse intensities along specific longitude ranges within the pulse window. The frequency peak of the amplitude corresponds to P_3 , while the phase variations across the pulse window, corresponding to the peak amplitude, give a more detailed indication of the subpulse motion across the window compared to P_2 . The periodic subpulse variations can be broadly categorised into two classes : phase modulated drifting which is associated with subpulse motion and periodic amplitude modulation, similar to periodic nulling, which is expected to be a different phenomenon distinct from sub-

pulse drifting (Basu *et al.* 2016; Mitra & Rankin 2017; Basu *et al.* 2017; Basu & Mitra 2018b). Phase modulated drifting also shows a wide variety of features which can be characterised by their drifting phase variations. For instance, positive drifting corresponds to the case where the phases show a decreasing trend from the leading to the trailing edge of the profile, and vice versa for negative drifting.

Subpulse drifting has been a topic of intensive research with the phenomenon expected to be present in 40-50% of the pulsar population. There are around 120 pulsars known at present to exhibit some form of periodic modulations in their single pulse sequence (Weltevrede *et al.* 2006, 2007; Basu *et al.* 2016). The drifting effects are very diverse and associations are seen with other phenomena like mode changing and nulling in some cases (Wright & Fowler 1981; Deich *et al.* 1986; Hankins & Wolszczan 1987; Vivekanand & Joshi 1997; Redman *et al.* 2005; Basu & Mitra 2018b). However, to gain a deeper understanding of the phenomenon at large, more comprehensive studies involving classification of the drifting population and identification of underlying traits are essential. The first such attempt was undertaken by Rankin (1986) who estimated the drifting behaviour within the empirical core-cone model of the emission beam. The pulsar profile, which is formed after averaging several

thousand single pulses, has a highly stable structure and is made up of one or more (typically 5) components. The components can be classified into two distinct categories, the central core component and the adjacent conal components. A number of detailed studies suggest that the radio emission beam consists of a central core emission surrounded by conal emission arranged in nested rings (Rankin 1990, 1993; Mitra & Deshpande 1999). The differences in the observed profiles are a result of the different line of sight (LOS) traverses across the emission beam. Rankin (1986) suggested subpulse drifting to be primarily a conal phenomenon, and the drifting to arise due to the circulation of the conal emission around the magnetic axis. This would result in an association between the drifting properties (particularly the phase variation of the drifting feature across the pulse) and the profile classification. The most prominent drifting with clear drift bands and large phase variations was associated with the conal single (S_c) and barely resolved conal double (D) profile classes. This corresponded to the LOS traversing the emission beam towards the outer edge. Progressively more interior LOS traverses of the emission beam result in well resolved conal double (D), conal Triple (cT) and conal Quadruple (cQ) profile shapes. In the above classification scheme such profile classes were expected to show primarily longitude stationary drift with very little phase variations. The core dominated profiles were associated with central LOS traverses of the emission beam. The principal profile classes were categorised as core single (S_c), Triple (T) with a central core component and pair of conal outriders, and Multiple (M) with central core and two pairs of conal components. Subpulse drifting was expected to be phase stationary and only seen in the conal components of the T and M class profiles. However, the core components sometimes show longer periodic structures which were not classified as subpulse drifting.

A second classification scheme for subpulse drifting was introduced by Weltevrede *et al.* (2006, 2007) for their large drifting survey involving 187 pulsars. These studies primarily employed the fluctuation spectrum method to quantify the subpulse drifting features and identified periodic phenomena in around 55% of the pulsars studied. Subpulse drifting was categorised based on the peak frequency in the fluctuation spectrum with three primary drifting classes. The class “coherent” drifters had narrow features with widths smaller than 0.05 cycles/ P (where P corresponds to the pulsar period). The class “diffuse” drifters had wider features compared to “coherent” drifters and were further subdivided into two categories. The subclass “Dif” pulsars had features which were clearly separated from the alias boundaries of 0 and 0.5 cycles/ P , while the subclass “Dif*” had features bordering either boundary. Additionally, a fourth class of pulsars with longitude stationary subpulse modulation were also observed but were not classified into the drifting population. In this classification scheme no information regarding the core-cone nature of the profile class was utilized and hence many pulsars with core components showing low frequency features were also identified as subpulse drifters.

The Meterwavelength Single-pulse Polarimetric Emission Survey (MSPES) was conducted recently to characterise the single pulse behaviour of 123 pulsars (Mitra *et al.* 2016). The periodic subpulse behaviour was investigated by Basu *et al.* (2016) with 56 pulsars showing some form of periodicity. No classification studies of drifting was carried out in this work. But the study reported a clear separation between pulsars with prominent drift bands and periodic amplitude modulations. It was observed that the phase modulated drifting associated with the conal profiles showed a negative correlation between the drifting periodicity and the spin-down energy loss (\dot{E}). The periodic amplitude modulation had large peri-

odicities, in excess of $10P$ and did not show any dependence on \dot{E} . It was further shown by Basu *et al.* (2017) that the periodic amplitude modulation had similarities with the periodic nulling seen in certain pulsars, indicating a possible common origin for the two phenomena. A number of pulsars with periodic nulling have conal profiles which opens up the possibility that the low frequency features are not limited to core components only. These works provide physical basis for the assertion made by Rankin (1986) that subpulse drifting is primarily a conal phenomenon and the low frequency periodic modulation seen in the core components belongs to a different physical phenomenon. However, there are certain issues that have not been addressed in the MSPES studies. Firstly, drifting features of the conal components in core dominated profiles show relatively flatter phase variations. In the above works these drifting cases have not been clearly distinguished from periodic amplitude modulation in core components. Secondly, no detailed phase variation studies associated with subpulse drifting were reported. Finally, in order to estimate the P_3 dependence on \dot{E} , the sparking model of drifting as suggested by Ruderman & Sutherland (1975, hereafter RS75) was used. According to the RS75 model the radio emission emerges from an ultra-relativistic, outflowing plasma which is generated in an Inner Acceleration Region (IAR) above the polar cap. The IAR maintains a non-stationary flow of plasma via sparking discharges that undergo non-linear plasma instabilities around 500 km from the stellar surface to emit coherent curvature radio emission (Asseo & Melikidze 1998; Melikidze *et al.* 2000; Gil *et al.* 2004; Mitra *et al.* 2009). The subpulses are believed to be associated with each spark (Gil & Sendyk 2000), and the drifting occurs due to movement of sparks across the magnetic field in the IAR due to the $\mathbf{E} \times \mathbf{B}$ drift, where the electric field \mathbf{E} is the co-rotational electric field in the IAR. RS75 argued that in a pulsar where the rotation axis is anti-parallel to a star centered dipolar magnetic axis, as the sparks develop in the IAR, they move slower than the co-rotation speed. As a consequence with every rotation the sparks lag behind. Since the same effect is translated to the subpulse emission, an observer sees this effect as subpulse drifting. In a non-aligned rotator (where the dipole magnetic axis and rotation axis are not coincident), assuming that the spark motion is primarily due to the co-rotational electric field, the sparks motion is around the rotation axis. This gives a preferred direction for the subpulse motion within the pulse window from the leading to the trailing edge of the profile (Basu *et al.* 2016). This justifies the assumption that negative drifting correspond to the sparks lagging behind co-rotation speed with a periodicity greater than $2P$, while positive drifting is aliased and has periodicity between P and $2P$. However, it has been postulated that the magnetic field near the surface in the IAR is non-dipolar, while the magnetic field is strictly dipolar in the emission region (RS75, Gil *et al.* 2002; Mitra *et al.* 2009; Mitra 2017). This implies that even though the sparks lag behind co-rotation speed in the IAR, the corresponding subpulse motion does not necessarily exhibit a preferential direction within the pulse window, particularly for more central LOS traverses of the emission beam.

As mentioned earlier the phase variations of the drifting peaks give a more accurate diagnostic of the subpulse motion across the pulse window compared to P_2 . The possibility that the low frequency amplitude modulations can be associated with both core and conal emission makes the phase variation studies all the more important for categorising the drifting phenomenon in pulsars. However, only a handful of studies exist in the literature with detailed phase behaviour reported, for example Edwards *et al.* (2003); Rosen & Demorest (2011); Weltevrede (2016). Phase vari-

ations across the profile show considerable departure from linearity in a number of cases. A connection between non-linearity in phase variations and orthogonal polarization moding, especially for the outer cones, has been reported in Rankin & Ramachandran (2003); Rankin *et al.* (2005). A precursor study of the detailed phase behaviour associated with subpulse drifting in four pulsars has been conducted by Basu & Mitra (2018a). The primary objective of this paper is to extend this work and develop a uniform classification scheme for the subpulse drifting population. We have carried out extensive observations using the Giant Meterwave Radio Telescope (GMRT) as well as gathered archival data from the Telescope to characterise the subpulse drifting in the majority of pulsars where this phenomenon has been reported. The expanded sample is also useful for investigating the different physical relationships of the drifting population, particularly the dependence of P_3 on \dot{E} in the presence of non-dipolar magnetic fields in the IAR. In section 2 we report the details of the observations and analysis for both archival and recently acquired data. In section 3 we present the details of the drifting features including the classification scheme introduced in this work. In section 4 we discuss the physical properties of drifting in detail. Finally we summarize our results in section 5.

2 OBSERVATIONS AND ANALYSIS

Numerous detailed studies exist in the literature of individual pulsars exhibiting periodicity in their single pulse behaviour, however, there have been only a few major works collecting and enhancing this population. Rankin (1986) assembled all the available sources of periodic modulations, which at the time of their publication amounted to 40-50 pulsars. Weltevrede *et al.* (2006, 2007) considerably increased the drifting population and reported around 100 pulsars with periodic modulation, including most of the pulsars in the Rankin (1986) list. More recently Basu *et al.* (2016) incremented this population by around 20 sources in their MSPES studies using the GMRT. In this work we consider primarily the pulsars exhibiting subpulse drifting and not the periodic amplitude modulation which is considered to be a separate phenomenon. As mentioned earlier drifting is restricted to the conal components of pulsar profiles with core components not showing any signatures of this phenomenon. This is most evident in the T or M type profile classes where the drifting is seen primarily in the leading and trailing conal components with no signatures seen in the central core component (Mitra & Rankin 2008; Maan & Deshpande 2014). On the contrary periodic amplitude modulation is usually seen as a low frequency feature in the fluctuation spectrum. This phenomenon appears across both the core and the conal components simultaneously, at similar locations in the fluctuation spectrum, and is likely to be a result of changes in the conditions across the entire IAR. This is similar to the periodic nulling seen in certain pulsars which suggests a common physical origin for both (Basu *et al.* 2017). The low frequency feature seen in the fluctuation spectra has been interpreted in terms of a rotating-subbeam carousel pattern of the conal emission, which is sparsely populated and stable over several rotation periods (Herfindal & Rankin 2007, 2009; Force & Rankin 2010). Subpulse drifting arises due to circulation of beamlets, while the low frequency feature is expected to be indicative of overall circulation time. However, the presence of low frequency feature in core emission both in the form of amplitude modulation and periodic nulling strongly argues against this hypothesis. In certain pulsars where both these features are seen in the fluctuation spec-

tra, their shapes are very different which also indicates a different physical origin for the two phenomena (Basu *et al.* 2017).

In order to analyze the drifting features highly sensitive single pulse measurements are required. We have carried out a detailed study of the subpulse drifting population primarily using observations from the GMRT. Our objective was to determine the phase variations wherever possible and introduce a consistent classification scheme for drifting. The MSPES survey observed single pulses at two radio frequencies, 333 and 618 MHz, from a large number of pulsars primarily between 0° and -50° declinations (Mitra *et al.* 2016). The fluctuation spectral analyses for these sources were previously conducted by Basu *et al.* (2016). However, detailed phase variation estimates across the profile were only carried out for five pulsars from this list (Basu & Mitra 2018a,b). We have used the data from these observations to carry out more detailed phase variation studies of drifting. Additionally, we have also assembled archival observations carried out in the past, at 325 MHz for 50 pulsars on three separate occasions, 2004 August 27, 2006 February 14 and 2007 October 26. These observations recorded sensitive fully polarized single pulses using the now defunct GMRT hardware backend (Sirothia 2000). Detailed studies of polarization characteristics for many of these pulsars have been previously reported in Mitra & Rankin (2011), where the observing details as well as the instrumental setup are explained. However, no detailed fluctuation spectral studies of the single pulses were then carried out. We found several pulsars with drifting features which have also been included in this work. There were an additional 30-40 pulsars with periodic single pulse modulation particularly above 0° declination which were outside the archival sample. We have carried out new observations of around 35 pulsars using the GMRT, on seven separate occasions between November 2017 and January 2018, for a total time of 30 hours. These observations were carried out as a followup to MSPES. We recorded total intensity signals for roughly 2000 single pulses from each pulsar, at 333 MHz, with an observing setup similar to Basu & Mitra (2018a). We have compiled a list of 61 pulsars which is possibly the most complete database of subpulse drifting known at present. As mentioned earlier this list does not include the periodic amplitude modulation and periodic nulling cases.

We have used fluctuation spectral analysis to measure the drifting features. We employed analysis schemes similar to Basu & Mitra (2018a) in order to estimate the detailed phase behaviour corresponding to drifting. We estimated the Longitude Resolved Fluctuation Spectra (LRFS) using 256 consecutive single pulses, as well as their time variations by shifting the starting point by 50 pulses. The phase variations across the pulse window were estimated by fixing the phase to be zero at the longitude corresponding to peak amplitude in the average spectrum. This process was repeated for the entire pulse sequence, as detailed in Basu & Mitra (2018a). The Fourier transforms were estimated for each longitude and the phases were only calculated for significant detections (5σ baseline level) of the peaks at that longitude. This implied that in certain pulsars, with weak peaks in the fluctuation spectra, no phase information was available. In these cases we used the Harmonic Resolved Fluctuation Spectra (HRFS, Deshpande & Rankin 2001; Basu *et al.* 2016) to get indications of whether the drifting is positive or negative or roughly phase stationary. The phase studies reported here were carried out for pulsars which showed long durations of systematic subpulse drifting. In certain pulsars there is rapid mode changing and/or frequent long duration nulls, and the emission switches between multiple states, with or without subpulse drifting, at short intervals. These

require specialized techniques to separate emission modes and estimate drifting, and will be addressed in future works.

3 THE SUBPULSE DRIFTING CLASSES

Subpulse drifting has been classified in the past based on either the profile type or the width of the drifting feature. There are merits to both these schemes as although drifting is primarily a conal phenomenon there are clear differences seen between prominent drift bands and diffuse structures in the fluctuation spectra. We have classified pulsars into four groups based on the nature of their phase variations as well as the width of the drifting features. The criteria for these classifications are explained in detail below. In each pulsar we have also specified the profile class within the core-cone model of the emission beam as introduced by Rankin (1990, 1993). In some pulsars the profile types were not available in the literature and we have suggested possible profile types for the same based on their shapes and polarization properties.

3.1 Coherent phase modulated drifting

The most prominent drifting is characterised by visible drift bands in the single pulse sequence. Fluctuation spectra show the presence of sharp narrow peaks indicating highly structured drifting. The phases corresponding to the peak frequency show large systematic variations across the pulse window signifying large scale subpulse motion. All drifting features with time averaged widths, measured at full width at half maximum (FWHM), less than 0.05 cycles/ P , and phases varying monotonically for more than 100° across the majority of the pulse window have been classified as coherent phase modulated drifting. In Table 1 we report 23 pulsars which exhibit this drifting effect. In addition to the basic physical parameters, P and \dot{E} , the Table also shows the different emission modes, the drifting periodicity, the general direction of subpulse variation signified by positive (PD) and negative drifting (ND), and the profile classification for each pulsar. In many pulsars no previous profile classifications were available and our suggested classifications are marked with “*” in the Table. All the pulsars in this list exhibit conal profiles with the majority showing either S_d or D type profiles. There are 7 pulsars in this group that show the presence of mode changing with more than one stable emission state. The subpulse drifting changes in the different modes, with some modes showing no clear drift pattern.

In Appendix A we also show the fluctuation spectral plots for 12 pulsars, which include the time evolution of the LRFS as well as the phase and amplitude variation of the peak frequency across the pulse profile. The detailed phase variations for three pulsars in this group, J0820–1350 (B0818–13), J1555–3134 (B1552–31) and J1720–2933 (B1717–29) have been shown in Basu & Mitra (2018a). Pulsar J1555–3134 shows the presence of two distinct drifting peaks which are not harmonically related and likely suggests fast transitions between two different drift states. Pulsar J1727–2739 nulls for around 60% of the time and hence our analysis schemes were not suitable for estimating the detailed phase behaviour. However, the single pulse behaviour was studied in detail by Wen *et al.* (2016) who found the presence of three distinct emission modes during the burst phases, two of which show systematic drift motion with prominent drift bands. Additionally, pulsar J1822–2256 (B1819–22) has also been studied in detail, including the drifting behaviour, by Basu & Mitra (2018b). Pulsar J0946+0951 (B0943+10) has been extensively

studied (Deshpande & Rankin 2001) and shows the presence of large phase variations corresponding to sharp peaks in the fluctuation spectra. Pulsar J0459–0210 was part of our latest observations, but was affected by radio frequency interference (RFI) and could not be analyzed. In Weltevrede *et al.* (2007) the fluctuation spectra showed the presence of a narrow peak with preferred negative drifting. Two pulsars J1816–2650 (B1813–26) and J1919+0134 were observed in MSPES and their fluctuation spectra showed the presence of narrow peaks with preferred drift directions (Basu *et al.* 2016). However, their single pulses were not sensitive for the phase variation studies. In the case of PSR J1946+1805 (B1944+17) the emission is frequently interrupted by long nulls. Our analysis schemes were not adequate for estimating the detailed phase variations in this pulsar. However, the drifting properties have been investigated by Kloumann & Rankin (2010) and are consistent with the drifting class described here. It is also possible that the pulsar belongs to the switching phase-modulated drifting class described below and more detailed studies are required to estimate its phase variations. Finally, pulsar J2305+3100 (B2303+30) has prominent phase variations with a drifting periodicity very close to $2P$. The temporal fluctuations of the LRFS causes frequent switching between positive and negative drifting which smears out the average phase behaviour.

3.2 Switching phase modulated drifting

This group of pulsars is similar to the coherent phase modulated drifters with sharp peaks in their fluctuation spectra and large phase variations across the pulse window. The primary distinguishing feature involves a sudden switch in the phase variation across adjacent components. The pulsars where the FWHM of the drifting features, in the time averaged spectra, are less than 0.05 cycles/ P , and the phase variations either show reversals in slope or sudden 180° jumps in adjacent components, are classified as switching phase-modulated drifting. The three pulsars J0815+0939, J1034–3224 and J1842–0359 (B1839–04) where detailed phase variation studies show the presence of the rare phenomenon of bi-drifting, i.e. the positive and negative drift directions are seen simultaneously at different regions of the pulse window, are included in this classification scheme. In Table 2 we list the 7 pulsars which belong to this group, including their P , \dot{E} , different emission modes, drifting periodicity and profile classification. Once again we have marked with “*” our suggestions for the pulsars without previous profile classifications. As shown in the Table most of the pulsars in this group belong to cQ profile class, with four conal components, the only exception being J0323+3944 (B0320+39) which likely has cT profile shape. Additionally, pulsar J1034–3224 also has a low level preceding pre-cursor component which does not exhibit any detectable drifting (Basu *et al.* 2015; Basu & Mitra 2018a). Incidentally, all three bi-drifting pulsars as well as PSR J0820–4114 (B0818–41) have large profile widths of 100° longitude or more, suggesting small inclination angles between the rotation and magnetic axes.

Pulsar J0815+0939 shows positive drifting only in the second component while the remaining components show negative drifting (Champion *et al.* 2005; Szary & van Leeuwen 2017). In PSR J1034–3224 alternate components have opposite direction of phase variation, with the first and third components showing negative drifting and the second and fourth showing positive (Basu & Mitra 2018a). In case of J1842–0359 the leading part shows phase variation corresponding to negative drifting which reverses direction towards the middle into positive drift-

Table 1. The coherent phase modulated drifting

	PSRJ	PSRB	P (s)	\dot{E} (10^{30} erg s $^{-1}$)	Mode	P_3 (P)	Type	Profile	
1	J0034–0721	B0031–07	0.943	19.2	A B C	13±1 6.5±0.5 4.0±0.5	ND	S_d	A1, A2
2	J0108+6608	B0105+65	1.284	244	—	2.04±0.08	PD	S_d	A3
3	J0151–0635	B0148–06	1.465	5.56	—	14.4±0.8	ND	D	A4, A5
4	J0421–0345	—	2.161	4.55	—	3.1±0.1	PD	*D/ S_d	A6
5	J0459–0210	—	1.133	37.9	—	2.36±0.01	ND	*D	—
6	J0814+7429	B0809+74	1.292	3.08	—	11.1±0.1	ND	S_d	A7
7	J0820–1350	B0818–13	1.238	43.8	—	4.7±0.1	ND	S_d	[1]
8	J0934–5249	B0932–52	1.445	60.9	—	3.9±0.2	ND	S_d	A8
9	J0946+0951	B0943+10	1.098	104	B Q	2.15±0.01 —	PD —	S_d S_d -PC	[2]
10	J1418–3921	—	1.097	26.6	—	2.49±0.03	PD	*D	A9
11	J1543–0620	B1540–06	0.709	97.4	—	3.01±0.05	PD	S_d	A10
12	J1555–3134	B1552–31	0.518	17.7	Peak1 Peak2	17.5±3.6 10.2±1.0	ND	*D	[1]
13	J1720–2933	B1717–29	0.620	123	—	2.452±0.006	ND	* S_d	[1]
14	J1727–2739	—	1.293	20.1	A B C	9.7±1.6 5.2±0.9 —	ND —	*D	[3]
15	J1816–2650	B1813–26	0.593	12.6	—	4.1±0.2	ND	*D	—
16	J1822–2256	B1819–22	1.874	8.12	A Trans A B C	19.6±1.6 14.3±1.8 — 10.7±1.1	ND —	*D	[4]
17	J1901–0906	—	1.782	11.4	—	3.05±0.09	ND	*D	A11, A12
18	J1919+0134	—	1.604	5.63	—	6.6±0.6	ND	*D	—
19	J1921+1948	B1918+19	0.821	63.9	A B C N	6.1±0.3 3.8±0.1 2.45±0.04 —	PD —	c T	A13
20	J1946+1805	B1944+17	0.441	11.1	A B C D	13.8±0.7 6.1±1.7 — —	ND —	c T	—
21	J2046–0421	B2043–04	1.547	15.7	—	2.75±0.04	PD	S_d	A14, A15
22	J2305+3100	B2303+30	1.576	29.2	B Q	2.05±0.05 ~3	PD/ND	S_d	—
23	J2313+4253	B2310+42	0.349	104	—	2.1±0.1	PD	* c T	A16

*-These classifications were not available previously and suggested here.

1-Basu & Mitra (2018a); 2-Deshpande & Rankin (2001); 3-Wen *et al.* (2016); 4-Basu & Mitra (2018b).

Table 2. The switching phase modulated drifting

	PSRJ	PSRB	P (s)	\dot{E} (10^{30} erg s $^{-1}$)	Mode	P_3 (P)	Profile	
1	J0323+3944	B0320+39	3.032	0.9	—	8.5 ± 0.3	* _c T	B1
2	J0815+0939	—	0.645	20.4	—	16.6 ± 0.3	* _c Q	[1]
3	J0820–4114	B0818–41	0.545	4.60	—	18.5 ± 1.5	_c Q	[2]
4	J1034–3224	—	1.151	5.97	—	7.2 ± 0.5	* _c Q	[3]
5	J1842–0359	B1839–04	1.840	3.22	—	12.4 ± 0.5	* _c Q	[4], B2
6	J1921+2153	B1919+21	1.337	22.3	—	4.2 ± 0.2	_c Q?	B3
7	J2321+6024	B2319+60	2.256	24.2	A B ABN	8 ± 1 4 ± 1 3 ± 0.5	_c Q	B4

*-These classifications were not available previously and suggested here.

1-Champion *et al.* (2005); Szary & van Leeuwen (2017); 2-Bhattacharyya *et al.* (2007, 2009); 3-Basu & Mitra (2018a); 4-Weltevrede (2016).

ing (Weltevrede 2016). Our analysis at 618 MHz is shown in Appendix B and also indicates a reversal in phase between the leading and trailing components. The phase behaviour of pulsar J0323+3944 has been shown in detail in Appendix B. An 180° phase jump has been previously reported (Edwards *et al.* 2003) for this pulsar near the center of the profile which is also seen in our plots. Pulsar J0820–4114 was observed as part of MSPES, but the detected single pulses were not sensitive for estimating drifting behaviour. However, the pulsar has been studied in detail by Bhattacharyya *et al.* (2007, 2009) who report that the central region shows a different subpulse motion compared to the outer components. It appears that no reversal in the drift direction is seen in the different components but more detailed phase variation studies would be required. Pulsar J1921+2153 (B1919+21) was observed in MSPES at 618 MHz and we have carried out detailed phase variation studies as shown in Appendix B. A jump in the phase variation is seen towards the center signifying different subpulse motion between the inner and outer parts of the profile. Finally, pulsar J2321+6024 (B2319+60) has been reported to exhibit three distinct drift modes by Wright & Fowler (1981). Our drifting analysis could only estimate the phase variations corresponding to the most dominant mode with $P_3 = 8P$ as shown in Appendix B. The phase variations show positive drifting, and no drift reversals are seen in any of the components. But a clear shift in the phase variations is seen between the adjacent second and third components which justifies the classification.

3.3 Diffuse phase modulated drifting

This group of pulsars exhibits wide structures in their fluctuation spectra which indicate the presence of multiple drift bands in the emission. Pulsars with FWHM of drifting features greater than 0.5 cycles/ P in the time average fluctuation spectra and no clearly measurable phase variations, but a clear preference for a drift direction, are identified as diffuse phase modulated drifters. A notable example of this phenomenon has been recently seen in the B mode of the pulsar J1822–2256 by Basu & Mitra (2018b). The single pulse behaviour shows the presence of multiple short lived subpulse tracks with the fluctuation spectra showing a wide structure without any

distinct peaks. In Table 3 we have assembled 15 pulsars which exhibit wide structures in their fluctuation spectra. The individual drift bands usually have short durations, so have no significant peaks in their average spectra. As a result the average phase behaviour cannot be determined using the techniques employed in this work. However, as described in Basu *et al.* (2016) the harmonic spectrum gives an indication of the general nature of the drift direction. Negative drifting is seen in the 0–0.5 cycles/ P region of the HRFS while for positive drifting the peak structure is shifted into the 0.5–1 cycles/ P region. In addition to P and \dot{E} the Table also lists mean drifting periodicity, drifting type and classification of the profile, including ‘*’ identifiers for newly suggested classifications.

As indicated in the Table the fluctuation spectral studies have been reported earlier for 12 pulsars, 9 pulsars in Basu *et al.* (2016), PSR J0630–2834 (B0628–28), J1703–1846 (B1700–18) and J1720–0212 (B1718–02) in Weltevrede *et al.* (2007) and J1840–0840 in Gajjar *et al.* (2017). For two pulsars J0823+0159 (B0820+02) and J2018+2839 (B2016+28) we have carried out new measurements for the fluctuation spectra as shown in Appendix C. Pulsar J2018+2839 is particularly interesting since the wide peak corresponding to drifting fills up the entire window between 0–0.5 cycles/ P in the average LRFS. Short duration drift bands are also prominently seen in its single pulse sequence. It should be noted that the wide structures seen in these pulsars are different from the temporal fluctuations of the single drifting peaks reported in Basu & Mitra (2018a). The closest counterpart is the two peaks seen in the fluctuation spectra of PSR J1555–3134, where the drifting is likely to alternate between two different states at rapid intervals.

3.4 Low-mixed phase-modulated drifting

This group comprises pulsars which have been previously identified as exhibiting phase-stationary drifting, where the subpulses are not expected to move across the pulse window but show periodic fluctuations in intensity. These pulsars usually show the presence of a central core component in their profiles which does not exhibit any drifting feature. However, our detailed studies reveal that in many of these cases the phases are not stationary across the profile

Table 3. The diffuse phase modulated drifting

	PSRJ	PSRB	P (s)	\dot{E} (10^{30}erg s^{-1})	P_3 (P)	Type	Profile	
1	J0152–1637	B0149–16	0.833	88.8	5.9 ± 1.0	ND	D	[1]
2	J0304+1932	B0301+19	1.388	19.1	6.4 ± 1.7	ND	D	[1]
3	J0525+1115	B0523+11	0.354	65.3	3.2 ± 0.5	PD	*D	[1]
4	J0630–2834	B0628–28	1.244	146	6.9 ± 1.5	PD	S_d	[2]
5	J0823+0159	B0820+02	0.865	6.38	4.7 ± 0.6	PD	* S_d	C1
6	J0944–1354	B0942–13	0.570	9.63	6.4 ± 0.3	ND	* cT	[1]
7	J0959–4809	B0957–47	0.670	10.8	5.6 ± 1.3	ND	D	[1]
8	J1041–1942	B1039–19	1.386	14.0	4.3 ± 0.4	PD	* cT	[1]
9	J1703–1846	B1700–18	0.804	131	3.6 ± 0.2	ND	* S_d	[2]
10	J1720–0212	B1718–02	0.478	30.0	5.4 ± 0.1	PD	*D	[2]
11	J1741–0840	B1738–08	2.043	10.5	4.6 ± 0.6	PD	$cQ?$	[1]
12	J1840–0840	—	5.309	6.25	15.0 ± 0.8	PD	*D	[3]
13	J2018+2839	B2016+28	0.558	33.7	4.0 ± 0.2	ND	S_d	C2
14	J2046+1540	B2044+15	1.138	4.88	23.0 ± 6.1	ND	D	[1]
15	J2317+2149	B2315+21	1.445	13.7	5.2 ± 0.4	ND	cT	[1]

*-These classifications were not available previously and suggested here.

1-Basu *et al.* (2016); 2-Weltevrede *et al.* (2007); 3-Gajjar *et al.* (2017);

but show significant variations, though these variations are lower compared to the coherent phase-modulated pulsars. We have classified pulsars which show relatively shallow phase variations of less than 100° across different components of the profile as low-mixed phase-modulated drifting. The mixed nature reflects the fact that in certain components the phase variations have opposite slopes. However, the extent of these variations is significantly lower than the switching phase-modulated drifters. The FWHM of the drifting feature in the fluctuation spectra varies for different pulsars in this group as well, similar to the coherent and diffuse classes described above, and possibly can be subdivided into two groups. However, the presence of the core component, along with lower phase variations identify this group. In Table 4 we list 16 pulsars including their P , \dot{E} , drifting periodicity and profile classification. Pulsars with periodic behaviour of the core component are believed to exhibit a different phenomenon and are not included in this list.

In Appendix D we show the detailed phase variations across the profile for 9 pulsars in this list. As mentioned above the phase variations are only seen in the conal components, with the variations much flatter than the coherent and switching phase modulation cases. However, even in these cases the phase variations are not zero but show curved trajectories. This implies that even for central LOS traverses through the emission beams the conal components show subpulse motion across the pulse window, which is smaller than the more peripheral traverse. Pulsar J0837+0610 (B0834+06) has a D profile and is the only one in this list with

out the presence of any clear core component. However, the presence of relatively shallow phase variations of less than 50° across its two components prompted its drifting classification. In pulsar J1700–3312 we were not able to estimate the phase behaviour due to the lower sensitivity of the single pulses. However, the presence of a possible core component and the low drifting periodicity around $2P$ justified its classification. More sensitive single pulse studies are required to estimate the phase variations in this pulsar. In the case of three pulsars J1703–3241 (B1700–32), J1740+1311 (B1737+13) and J2048–1616 (B2045–16) the drifting exhibited wide features, with FWHM in excess of 0.05 cycles/ P , without any prominent single drifting periodicity, similar to the diffuse phase modulation case. Hence, no clear phase variation studies could be carried out for these pulsars, but detailed fluctuation spectra for these sources have been reported in Basu *et al.* (2016). In each of these pulsars it is clear that the drifting is restricted to the conal regions only. We did not have access to single pulses from the pulsar J1912+2104 (B1910+20) and could not estimate the phase variations. The pulsar has been studied by Weltevrede *et al.* (2007) where a low periodicity drifting feature is seen for only the leading conal component. Finally, two pulsars J1801–2920 (B1758–29) and J2006–0807 (B2003–08) also show the presence of drifting features in the fluctuation spectra associated with only the conal components (Basu *et al.* 2016). However, their single pulse behaviour is also characterized by frequent nulls which renders our analysis techniques inadequate for phase variation studies. These

Table 4. The low-mixed phase-modulated drifting

	PSRJ	PSRB	P (s)	\dot{E} (10^{30}erg s^{-1})	P_3 (P)	Profile	
1	J0624–0424	B0621–04	1.039	29.2	2.05 ± 0.01	M	D1
2	J0837+0610	B0834+06	1.274	130	2.17 ± 0.03	D	D2, D3
3	J0846–3533	B0844–35	1.116	45.5	2.03 ± 0.02	*M	D4, D5
4	J1239+2453	B1237+25	1.382	14.3	2.8 ± 0.1	M	D6, D7
5	J1328–4921	B1325–49	1.479	7.45	3.4 ± 0.2	*M _c Q	D8, D9
6	J1625–4048	—	2.355	1.34	61 ± 30	*T _c T	D10
7	J1650–1654	—	1.750	23.6	2.6 ± 0.1	*D/T	D11
8	J1700–3312	—	1.358	74.2	2.2 ± 0.1	*M	—
9	J1703–3241	B1700–32	1.212	14.6	4.7 ± 0.5	T	—
10	J1733–2228	B1730–22	0.872	2.55	23 ± 13	*T	D12
11	J1740+1311	B1737+13	0.803	110	9 ± 1	M	—
12	J1801–2920	B1758–29	1.082	103	2.48 ± 0.08	*T	—
13	J1900–2600	B1857–26	0.612	35.2	7.6 ± 0.8	M	D13, D14
14	J1912+2104	B1910+20	2.233	36.1	2.70 ± 0.04	MT?	—
15	J2006–0807	B2003–08	0.581	9.27	15.2 ± 2.5	M	—
16	J2048–1616	B2045–16	1.962	57.3	3.23 ± 0.03	T	—

*-These classifications were not available previously and suggested here.

would require a separate analysis scheme where the burst regions are separated out and drifting analysis is carried out on individual segments.

4 DISCUSSION

4.1 The effect of Aliasing and dependence on Spin-down energy loss

As discussed in the introduction, the RS75 model, which postulates that the sparking discharges in the IAR lag behind co-rotation speed, has been used to unravel the aliasing associated with subpulse drifting. This gives a natural solution for estimating the alias where negative drifting has periodicities in excess of $2P$, and positive drifting has periodicities less than $2P$. This was used to determine a dependence between the drifting periodicity and spin-down energy loss (\dot{E}) which exhibits a negative correlation (Basu *et al.* 2016). However, there are some issues with the above assumptions. Firstly, a number of pulsars like the switching phase-modulated and low-mixed phase-modulated drifters do not show any specific drift direction. Secondly, the magnetic field structure in the IAR is highly non-dipolar in nature, while the magnetic field in the emission region is dipolar (Mitra 2017). This ensures that the spark tracks in the non-dipolar IAR which lag behind co-rotation speed will have more convoluted subpulse motion in the emission

region due to the transition of the magnetic fields from the non-dipolar to dipolar. This still does not justify a carousel like motion of subpulses as proposed in certain models (Gil & Sendyk 2000; Deshpande & Rankin 2001), as the subpulse motion in this model requires the sparks to lag behind co-rotation speed in certain instances and lead co-rotation speed in others. A more detailed model of subpulse drifting needs to be explored to understand the observational results. But, we once again take a detailed look into the dependence of P_3 on \dot{E} for the extended sample studied here. In Figure 1, left panel, we have plotted P_3 as a function of \dot{E} for all 61 pulsars which are expected to exhibit subpulse drifting. The four different drifting classes are represented separately in the Figure. We have not resolved the alias using the drift direction and have used periodicities $>2P$ for all measurements. On the right panel we have isolated only the coherent drifting pulsars which are mainly associated with LOS cuts of the emission beam towards the edge of the profile. These are less likely to be affected by non-dipolar effects of the inner field lines. Similar to Basu *et al.* (2016) we have resolved the alias around $2P$ by assuming that negative drifting has $P_3 >2P$ and positive drifting has $P_3 <2P$. As seen in the left panel of the Figure, despite a large scatter there exists a dependence between the two quantities with P_3 increasing with decreasing \dot{E} . The dependence flattens out between 10^{31} and 10^{32} erg s⁻¹ where P_3 s are likely to be aliased. This is further highlighted by the fact that most P_3 values close to $2P$ boundary appear in this range. The

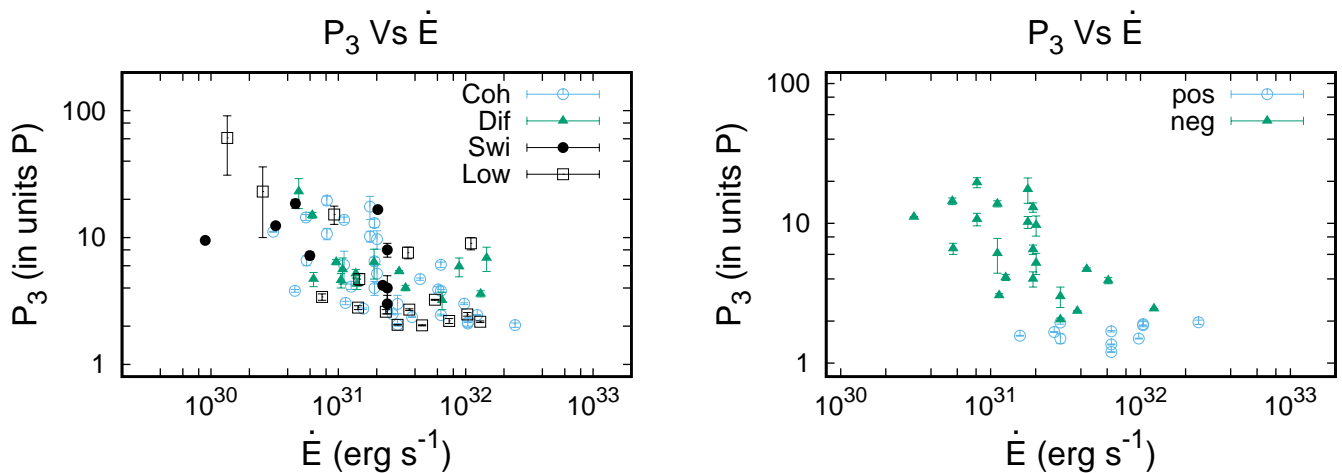


Figure 1. The Figure shows the variation of the drifting periodicity P_3 as a function of the spin-down energy loss (\dot{E}). The left panel shows all pulsars with subpulse drifting with the four different classes of drifting separately indicated in the Figure. The right panel only shows the coherent drifting class associated with peripheral line of sight cuts of the emission beam. The alias around $2P$ is resolved by assuming $P_3 > 2P$ for negative drift directions and $P_3 < 2P$ for positive drifting.

correlation becomes even more prominent on the right panel where we are dealing with cleaner examples of systematic subpulse drifting.

4.2 The Pulsars without subpulse drifting

As noted earlier drifting is primarily a conal phenomenon and hence core dominated pulsars belonging to the S_t and T profile classes, with weak or absent conal emission, do not show any drifting. However, the low frequency features associated with periodic amplitude modulation or nulling are seen in a number of these pulsars. Additionally, there are also many pulsars with prominent conal emission where detailed studies have not revealed any measurable drifting features. In Table 5 we have listed 69 pulsars with distinct conal components which do not show any drifting, along with their \dot{E} and profile classifications. There are 23 pulsars in this list with $\dot{E} > 5 \times 10^{32}$ erg s $^{-1}$ and the remaining 46 are below this limit. There are also around 100 pulsars with profile classifications where the single pulses are too weak to carry out detailed analysis.

One primary feature of drifting studies reported in this work is that the majority of measurements are carried out at a single frequency of 325 MHz. This however makes it difficult to estimate frequency evolution of the drifting phenomenon particularly at higher frequencies. It has been observed that the conal emission in core dominated pulsars becomes more prominent at higher frequencies (Rankin 1983; Mitra & Rankin 2017). It is possible that some core dominated pulsars show subpulse drifting in their conal components at higher frequencies. But a majority of such pulsars have \dot{E} greater than 10^{33} erg s $^{-1}$ making it unlikely for drifting to be seen. Detailed single pulse observations at frequencies in excess of 2 GHz would be required to address this issue. There are 46 pulsars where sensitive single pulse studies show no drifting. This implies that drifting is seen in 57% of pulsars with conal emission and $\dot{E} < 5 \times 10^{32}$ erg s $^{-1}$. As seen in the Table non-drifting pulsars are not restricted to any specific profile class. It is not clear at present why a large fraction of conal pulsars do not show presence of drifting. One possibility is that the absence of drifting is an extreme example of diffuse drifting category where the pulsar switches rapidly be-

tween multiple subpulse tracks. In absence of any apparent physical characteristics distinguishing between the two populations, more detailed modelling is essential to better understand the conditions affecting the drifting phenomenon.

4.3 The Conal emission in Pulsars

There are no cases of drifting with $\dot{E} > 5 \times 10^{32}$ erg s $^{-1}$ which has also been noted previously in Basu *et al.* (2016). It has also been established that drifting is primarily a conal phenomenon. This raises the question about whether the different profile classes have similar dependencies on \dot{E} . As mentioned earlier profile classifications were introduced in the works of Rankin (1990, 1993). Detailed profile classifications for the MSPES pulsars were carried out by Skrzypczak (2017). There are around 300 pulsars with classifications, and their distribution as a function of \dot{E} for 6 different classes S_d , S_t , D, cT , T and M are shown in Figure 2. The cT distribution also includes the cQ class since they both represent conal profiles with multiple components. The Figure shows a clear demarcation between core dominated profiles and conal pulsars. The \dot{E} of majority of conal pulsars belonging to the S_d and D classes lie below 10^{33} erg s $^{-1}$ while the core single profiles mostly have higher \dot{E} values. The differences become less clear in more complicated profile types (T, cT and M), though their numbers become lower at higher \dot{E} range. This gives a possible indication about absence of drifting in the higher \dot{E} range. These results highlight that the distinction between core and conal dominated profiles are not just a geometrical effect, related to the line of sight traverse through the emission beam, but also a likely outcome of other physical processes. In previous studies there have been indications of physical differences between profile classes. For example Rankin (1993) used B_{12}/P^2 as an indicator for core and conal species with the cores having larger values. Similarly, Gil & Sendyk (2000) introduced the complexity parameter to distinguish core and conal profile classes. It has been recently shown by Skrzypczak *et al.* (2018) that the underlying widths of core and conal components in profiles are similar and has a $P^{-0.5}$ dependence. In order to understand the physical processes leading to different profile classes more de-

Table 5. List of Pulsars with prominent conal components but no detectable drifting

Pulsar	\dot{E} (10^{30} erg s $^{-1}$)	Profile	Pulsar	\dot{E} (10^{30} erg s $^{-1}$)	Profile	Pulsar	\dot{E} (10^{30} erg s $^{-1}$)	Profile			
1	B0052+51	39.8	*D	26	B1530+27	21.6	S_d/D	51	B1845-01	723	cT
2	J0134-2937	1.20×10^3	* cT	27	B1541+09	40.7	T	52	J1850+0026	11.2	*M
3	B0138+59	8.44	M	28	B1558-50	4.26×10^3	T	53	J1857-1027	8.31	*T/ cT
4	B0144+59	1.34×10^3	*T	29	B1601-52	35.5	D	54	B1905+39	11.3	M
5	B0329+54	222	T/M	30	B1604-00	161	T	55	B1907+03	13.9	T/M
6	B0402+61	1.05×10^3	T/M	31	B1612+07	53.0	S_d	56	B1914+09	5.04×10^3	$T_{1/2}$
7	B0447-12	48.2	*M	32	B1633+24	39.9	cT	57	B1917+00	147	T
8	B0450-18	1.37×10^3	T	33	B1648-17	130	*D	58	B1923+04	78.3	S_d
9	B0450+55	2.37×10^3	T	34	B1649-23	25.2	* $T_{1/2}$	59	B1929+10	3.93×10^3	$T_{1/2}$
10	B0458+46	846	T	35	J1652+2651	33.6	*D	60	B2021+51	816	D/ S_d
11	J0520-2553	84.2	*D	36	B1717-16	59.6	*D	61	B2044+15	4.88	D
12	B0525+21	30.1	D	37	B1718-32	235	* $T_{1/2}$	62	B2110+27	59.5	S_d
13	B0559-05	828	*T	38	B1727-47	1.13×10^4	T	63	B2148+63	121	S_d
14	B0727-18	5.64×10^3	*T	39	B1742-30	8.49×10^3	T	64	B2154+40	38.2	cT/D
15	B0736-40	1.21×10^3	T	40	B1745-12	782	T/M	65	B2227+61	1.02×10^3	* cQ/M
16	B0740-28	1.43×10^5	T/M	41	B1747-46	125	T/M	66	B2306+55	73.5	D
17	B0751+32	14.2	D	42	B1753+52	4.52	*D	67	B2323+63	37.6	D/ cQ
18	B0905-51	4.43×10^3	* cQ/M	43	B1754-24	4.00×10^4	*T	68	B2327-20	41.2	T
19	B0919+06	6.79×10^3	T	44	B1758-29	103	*T	69	J2346-0609	32.6	*D
20	B0950+08	560	S_d	45	B1804-08	259	T				
21	B1133+16	87.9	D	46	J1808-0813	72.8	* S_d				
22	B1254-10	60.9	*D	47	B1821+05	21.0	T				
23	B1322+83	74.3	S_d	48	B1826-17	7.57×10^3	T				
24	B1508+55	488	T	49	B1831-04	116	M				
25	B1524-39	53.3	D	50	B1845-19	11.5	*T				

*-These classifications were not available previously and suggested here.

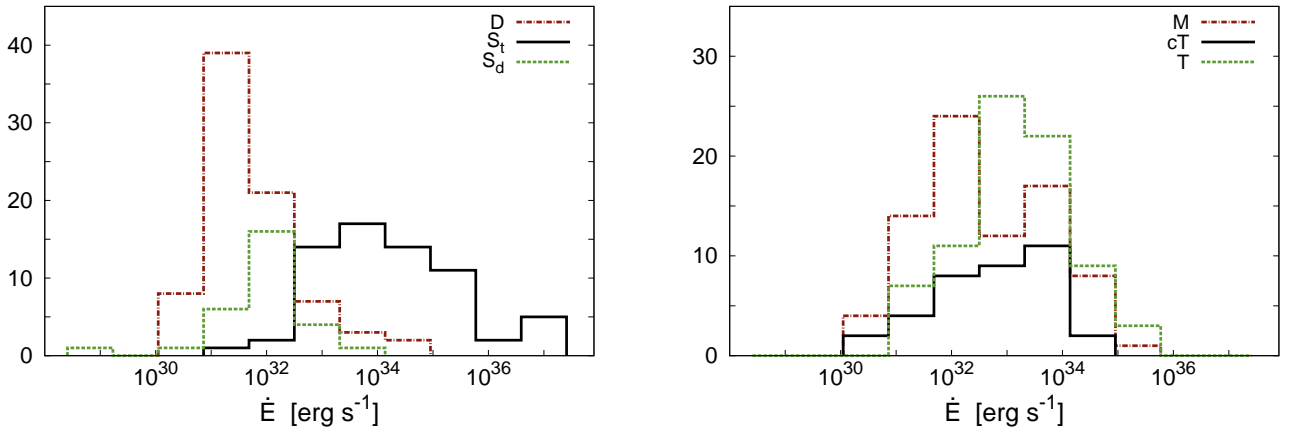


Figure 2. The Figure shows the distribution of the different profile classes as a function of the spin-down energy loss (\dot{E}). The left panel shows the distribution for the three profile classes, conal single (S_d), conal double (D) and core single (S_t). The right panel shows the distribution for the Multiple (M), Triple (T) and conal Triple (cT) profile classes. The cT class in this distribution is a combination of the conal Triple and conal Quadruple (cQ) classes.

tailed modelling is required. The dependence seen between P_3 and \dot{E} reported in this work should serve as an input into these models. One example is the partially screened gap (PSG) model where the IAR is screened by thermally emitted ions from the stellar surface (Gil *et al.* 2003; Szary *et al.* 2015). The drifting periodicity in this model is inversely proportional to screening factor of the gap and hence an inverse dependence of P_3 on \dot{E} can be established (Basu *et al.* 2016). However, this model needs to be extended to explain variations seen in the physical properties of core and conal pulsars.

4.4 The association between Drifting and Profile Classifications

A distinct association between the nature of subpulse drifting and profile class was noted by Rankin (1986). It was seen that the most ordered drifting was associated with the S_d class and barely resolved D profiles where the LOS was supposed to traverse the emission beam tangentially. On the contrary well resolved D profiles as well as conal components of the T and M profiles were not expected to drift but show pulse-to-pulse phase-stationary modula-

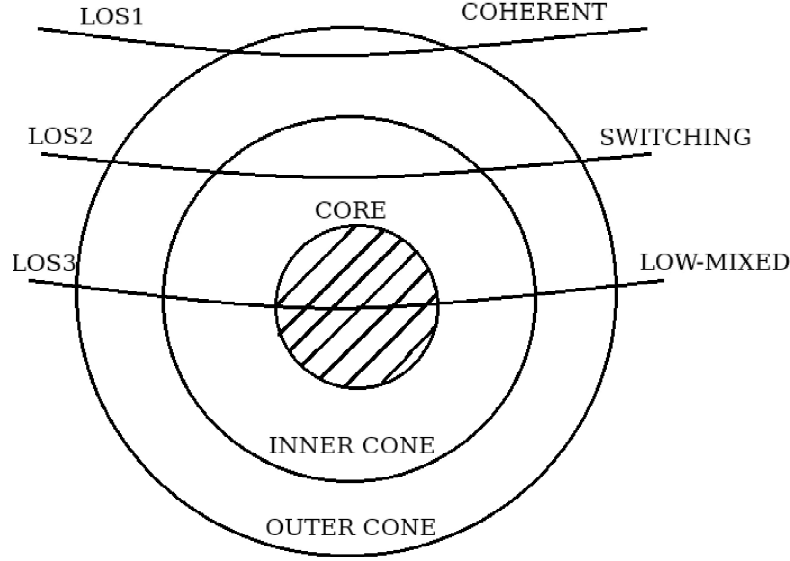


Figure 3. The Figure shows a schematic of the association of the different drifting classes with the line-of-sight (LOS) traverse of the emission beam. Coherent drifting with regular phase variations are associated with outermost LOS1. Switching phase-modulated drifting is usually associated with more interior LOS2. The central core region does not show any systematic subpulse drifting. Low-mixed phase-modulated drifting is associated with conal regions of central LOS3.

tion. This behaviour was interpreted as the LOS traversing emission beam more centrally, with conal radio emission circulating around magnetic axis. The presence of detailed phase variation measurements associated with drifting makes it appropriate to revisit this suggested association.

As shown in Table 1 the majority of pulsars which exhibit large and systematic phase variations across the profile are associated with S_d and barely resolved D profiles. The phases monotonically increase or decrease across the profile for several hundred degrees. However, as profile shapes become more complicated the drifting behaviour also show large diversity. Well resolved conal D profiles do not necessarily exhibit phase-stationary behaviour. For example in PSR J0837+0610 (B0834+06) the phase variations, particularly in the trailing component, are relatively flat with less than 20° variation. The pulsar has been classified in the low-mixed phase-modulated drifting category. In contrast a number of pulsars with D profiles show large phase variations across the components and have been classified in the coherent phase-modulated drifting class. The most prominent D class pulsars with clearly separated components are J0151–0635 (B0148–06), where the leading component exhibits between 100 – 150° phase variations and the trailing component between 50 – 100° ; and J1901–0906 where the drifting is prominent primarily in the trailing component with more than 200° phase variation across the component. In three pulsars J1921+1948 (B1918+19), J1946+1805 (B1944+17) and J2313+4253 (B2310+42) belonging to the cT profile class, the phases show more than several hundred degree variations across the profile and are classified as coherent phase-modulated drifters. Pulsar J0323+3944 (B0320+39) also shows similar large phase variations, but a 180° phase jump is seen towards the center of the profile. Due to its complex phase behaviour we have classified the profile as cT . For six cQ pulsars showing subpulse drifting, once again large phase variations exceeding several hundred degrees across the profiles are seen. However, in each of these pulsars phase variations show sudden jumps between components, which include the

three bi-drifting pulsars where slope of phase variations changes sign due to drift reversals. These pulsars along with J0323+3944 (B0320+39) have been identified as a separate class of switching phase-modulated drifting. Finally, the drifting in the conal components of T and M class profiles, in addition to PSR J0837+0610 (B0834+06), is identified as low-mixed phase-modulated drifting which is different from phase stationary behaviour. The phase variations are not strictly zero but show variations of 50° across certain components. The most prominent variations are seen in the inner cone of PSR J1239+2453 (B1237+25), as well as J1733–2228 (B1730–22) in its strong leading component.

In summary a general evolution of the phase variations corresponding to drifting is indeed seen with the pulsar profile class. The more conal profiles, S_d , D and cT are associated with tangential LOS cuts of the emission beam and show a systematic change in the phase variations across the profile components. In case of more inward LOS traverses, corresponding to cQ profile type and certain cT pulsars, the phase jumps and phase reversals become more prominent. Finally, for central LOS traverse corresponding to the M and T class profiles, the drifting is absent in the central core component while the conal components show relatively smaller phase variations, which however still show the complexity of the switching class. A schematic explaining the association of the different drifting categories with the LOS traverse of the emission beam is shown in the Figure 3. But it should be noted that the schematic is only representative of the generalized association between drifting behaviour, with profile class with clear deviations seen in individual pulsars. Estimation of the detailed emission geometry in each case would likely provide a better understanding of this association. There are a few possibilities for the deviation of the phase variations from linearity. A flattening of phases towards the peripheral longitudes is seen in a number of S_d pulsars. This can develop due to curvature of the LOS in more tangential traverses of the emission beam. In certain pulsars it has been shown that phase jumps are correlated with variations in the orthogonal polarization modes

(Rankin & Ramachandran 2003; Rankin *et al.* 2005), particularly for the outer conal components. This phenomenon needs to be explored in more detail by carrying out sensitive polarization modal studies in drifting pulsars. Finally, presence of non-dipolar surface fields in the IAR, as proposed by RS75, is another possible source of deviation from linear phase variations. The sparks, responsible for the outflowing plasma, undergo \mathbf{ExB} drift in the IAR in presence of highly curved non-dipolar magnetic fields. On the other hand the subpulses corresponding to the observed emission originate at regions associated with dipolar field lines (Mitra 2017). The transition from non-dipolar fields in the IAR to dipolar fields in the emission region is likely to lead to non-linearity in drifting phases. However, detailed modelling is required to understand the spark motion in the IAR.

5 SUMMARY

We have carried out a detailed analysis of subpulse drifting in pulsars and assembled the most complete sample exhibiting this phenomenon. We have made careful distinctions between drifting and other phenomena like periodic amplitude modulations and periodic nulling. We have used fluctuation spectral analysis to characterise the drifting features, particularly the nature of frequency peaks and phase variations across the profile associated with the peaks. Based on these measurements the drifting population was divided into four main categories: coherent phase-modulated drifting with narrow frequency features and regular phase variations across the profile; switching phase-modulated drifting with narrow frequency features but exhibiting sudden jumps and reversals in phase variations; diffuse phase-modulated drifting with relatively wide frequency features and indication of a drift direction; and low-mixed phase-modulated drifting associated with pulsars with central core components, which do not show drifting, and corresponding conal components, showing relatively lower but complex phase variations. The classification scheme introduced in this work differs from the previous schemes of Rankin (1986) and Weltevrede *et al.* (2006, 2007). In contrast to Rankin (1986) the classification is based not just on profile class but also the nature of subpulse drifting seen in each profile class. However, our classification uses the suggestion by Rankin (1986) that drifting is restricted to conal components, which was not utilized in the works of Weltevrede *et al.* (2006, 2007). Drifting periodicities are anti-correlated with spin-down energy loss (\dot{E}). It is also observed that drifting is restricted to a narrow range of $\dot{E} < 5 \times 10^{32} \text{ erg s}^{-1}$. The drifting classification shows an association with the profile types and line-of-sight (LOS) geometry. The coherent phase-modulated drifting is associated with S_d and barely resolved D profiles with tangential LOS traverses of the emission beam. The switching phase-modulated drifting is seen in more interior LOS traverses of c_T and c_Q pulsars. While the low-mixed phase-modulated drifting usually appears in T and M profiles with central LOS traverse.

ACKNOWLEDGMENTS

We thank the referee Prof. Joanna Rankin for her comments which helped to improve the paper. Dipanjan Mitra acknowledges funding from the grant ‘‘Indo-French Centre for the Promotion of Advanced Research - CEFIPRA’’. We thank the staff of the GMRT who have made these observations possible. The GMRT is run by

the National Centre for Radio Astrophysics of the Tata Institute of Fundamental Research.

REFERENCES

- Asseo, E.; Melikidze, G.I. 1998, MNRAS, 301, 59
 Backer, D.C. 1973, ApJ, 182, 245
 Backer, D.C.; Rankin, J.M.; Campbell, D.B. 1975, ApJ, 197, 481
 Basu, R.; Mitra, D.; Rankin J.M. 2015, ApJ, 798, 105
 Basu, R.; Mitra, D.; Melikidze, G.I.; Maciesiak, K.; Skrzypczak, A.; Szary, A. 2016, ApJ, 833, 29
 Basu, R.; Mitra, D.; Melikidze, G.I. 2017, ApJ, 846, 109
 Basu, R.; Mitra, D. 2018a, 475, 5098
 Basu, R.; Mitra, D. 2018b, 476, 1345
 Bhattacharyya, B.; Gupta, Y.; Gil, J.; Sendyk, M. 2007, MNRAS, 377, L10
 Bhattacharyya, B.; Gupta, Y.; Gil, J. 2009, MNRAS, 398, 1435
 Champion, D.J.; Lorimer, D.R.; McLaughlin, M.A.; Xilouris, K.M.; Arzoumanian, Z.; Freire, P.C.C.; Lommen, A.N.; Cordes, J.M.; Camilo, F. 2005, MNRAS, 363, 929
 Deich, W.T.S.; Cordes, J.M.; Hankins, T.H.; Rankin, J.M. 1986 ApJ, 300, 540
 Deshpande, A.A.; Rankin, J.M. 2001, ApJ, 322, 438
 Drake, F.D.; Craft, H.D. 1968, Nature, 220, 231
 Edwards, R.T.; Stappers, B.W.; van Leeuwen, A.G.J. 2003, A&A, 402, 321
 Force, M.M.; Rankin, J.M. 2010, MNRAS, 406, 237
 Gajjar, V.; Yuan, J.P.; Yuen, R.; Wen, Z. G.; Liu, Z. Y.; Wang, N. 2017, ApJ, 850, 173
 Gil, J.A.; Lyne, A.G. 1995, MNRAS, 276L, 55
 Gil, J.A.; Sendyk, M. 2000, ApJ, 541, 351
 Gil, J.A.; Melikidze, G.I.; Mitra, D. 2002, A&A, 388, 235
 Gil, J.A.; Melikidze, G.I.; Geppert, U. 2003, A&A, 407, 315
 Gil, J.; Lyubarsky, Y.; Melikidze, G.I. 2004, ApJ, 600, 872
 Hankins, T.H.; Wolszczan, A. 1987, ApJ, 318, 410
 Herfindal, J.L.; Rankin, J.M. 2007, MNRAS, 380, 430
 Herfindal, J.L.; Rankin, J.M. 2009, MNRAS, 393, 1391
 Kloumann, I.M.; Rankin, J.M. 2010, MNRAS, 408, 40
 Maan, Y., Deshpande, A.A. 2014, ApJ, 792, 130
 Melikidze, G.I.; Gil, J.A.; Pataraya, A.D. 2000, ApJ, 544, 1081
 Mitra, D., Deshpande, A.A. 1999, A&A, 346, 906
 Mitra, D.; Rankin, J. 2008, MNRAS, 385, 606
 Mitra, D.; Gil, J.; Melikidze, G. 2009, ApJL, 696, L141
 Mitra, D.; Rankin, J. 2011, ApJ, 727, 92
 Mitra, D.; Basu, R.; Maciesiak, K.; Skrzypczak, A.; Melikidze, G.I.; Szary, A.; Krzeszowski, K. 2016, ApJ, 833, 28
 Mitra, D.; Rankin, J. 2017, ApJ, 468, 4601
 Mitra, D. 2017, JApA, 38, 52
 Rankin, J.M. 1983, ApJ, 274, 333
 Rankin, J.M. 1986, ApJ, 301, 901
 Rankin, J.M. 1990, ApJ, 352, 247
 Rankin, J.M. 1993, ApJ, 405, 285
 Rankin, J.M.; Ramachandran, R. 2003, ApJ, 590, 411
 Rankin, J.M.; Ramachandran, R.; Suleymanova, S.A. 2005, A&A, 429, 999
 Redman, S.L.; Wright, G.A.E.; Rankin, J.M. 2005, MNRAS, 357, 859
 Rosen, R.; Demorest, P. 2011, ApJ, 728, 156
 Ruderman, M.A.; Sutherland, P.G. 1975, ApJ, 196, 51
 Sirothia, S. 2000, MSc thesis, Univ. of Pune
 Skrzypczak, A. 2017, Phd thesis, University of Zielona Góra
 Skrzypczak, A.; Basu, R.; Mitra, D.; Melikidze, G.I.; Maciesiak, K.; Koralewska, O.; Filothodoros, A. 2018, ApJ, 854, 162
 Szary, A.; Melikidze, G.I.; Gil, J. 2015, MNRAS, 447, 2295
 Szary, A.; van Leeuwen, J. 2017, ApJ, 845, 95
 Vivekanand, M.; Joshi, B. C. 1997, ApJ, 477, 431
 Weltevrede, P.; Edwards, R. T.; Stappers, B. W. 2006, A&A, 445, 243
 Weltevrede, P.; Edwards, R. T.; Stappers, B. W. 2007, A&A, 469, 607
 Weltevrede, P. 2016, A&A, 590, 109
 Wen, Z.G.; Wang, N.; Yuan, J.P.; Yan, W.M.; Manchester, R.N.; Yuen, R.; Gajjar, V. 2016, A&A, 592, 127

Wright, G.A.E.; Fowler, L.A. 1981, MNRAS, 101, 356

**APPENDIX A: THE COHERENT PHASE MODULATED
DRIFTING : FLUCTUATION SPECTRAL PLOTS**

**APPENDIX B: THE SWITCHING PHASE MODULATED
DRIFTING : FLUCTUATION SPECTRAL PLOTS**

**APPENDIX C: THE DIFFUSE PHASE MODULATED
DRIFTING : FLUCTUATION SPECTRAL PLOTS**

**APPENDIX D: THE PHASE STATIONARY DRIFTING :
FLUCTUATION SPECTRAL PLOTS**

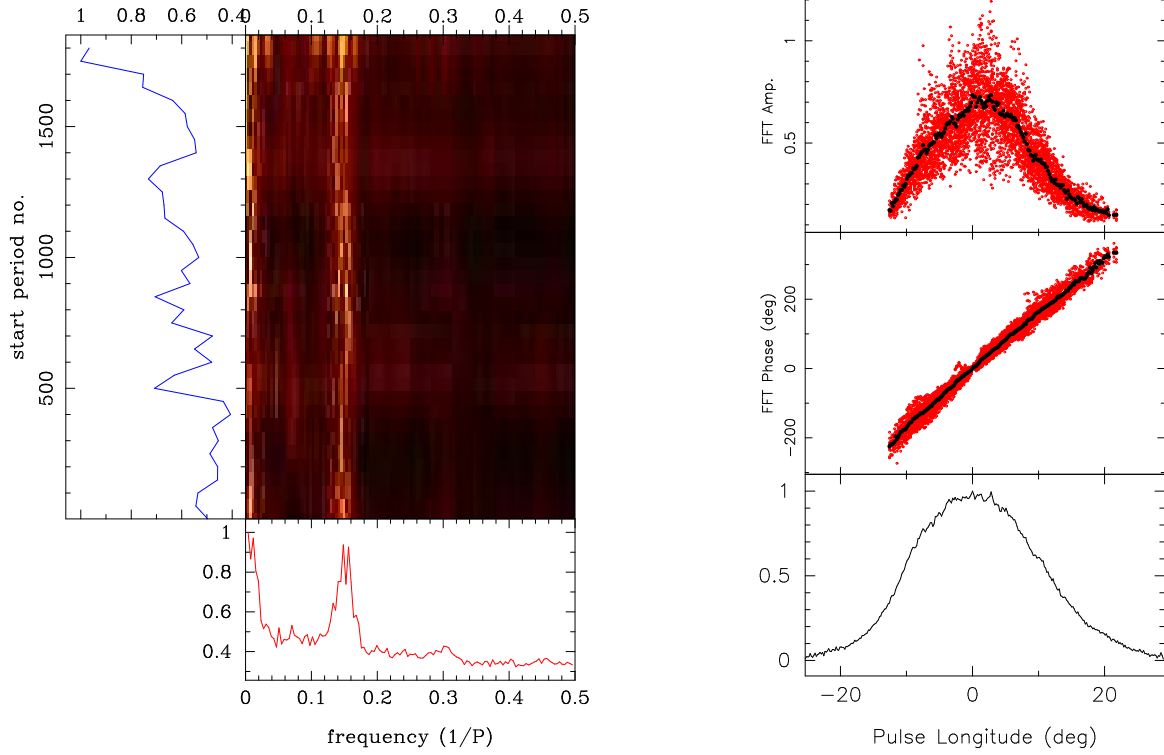


Figure A1. The fluctuation spectral analysis for PSR J0034–0721 at 333 MHz. The left panel shows time variation of LRFS. The right panel shows the variation of the peak frequency across the pulse window; peak amplitude (top window), phase variations (middle window), profile (bottom window).

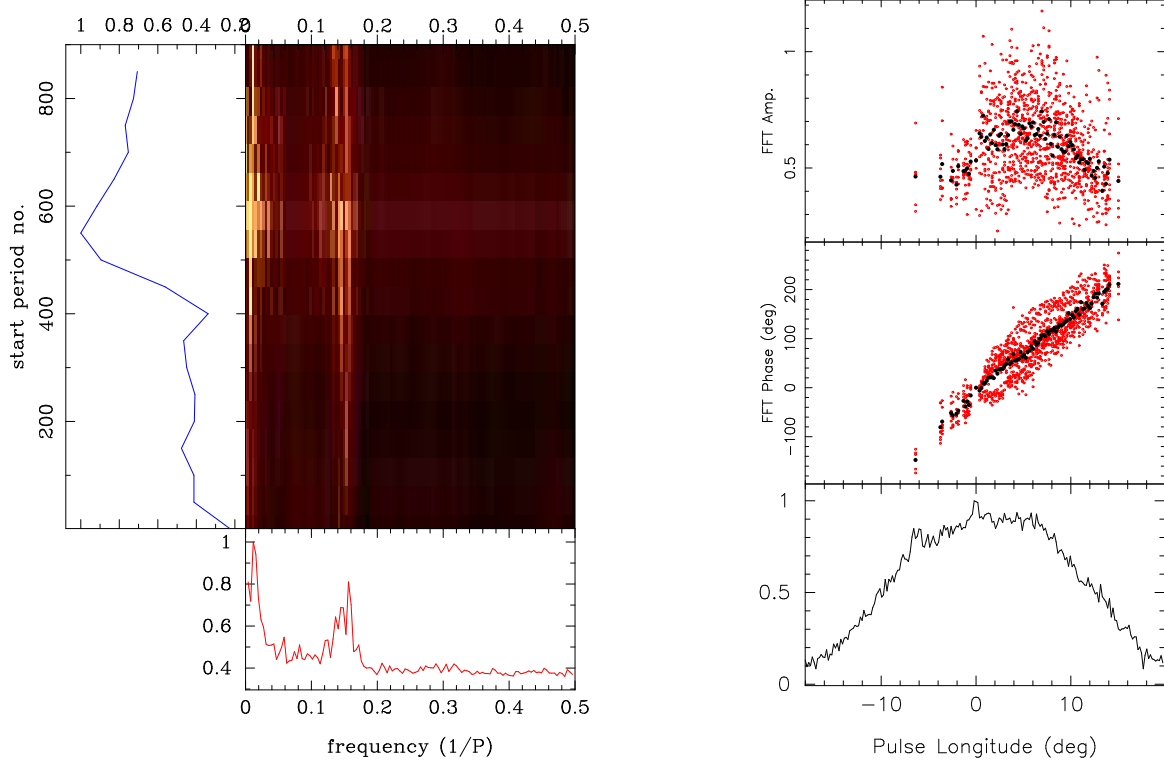


Figure A2. The fluctuation spectral analysis for PSR J0034–0721 at 618 MHz. The left panel shows time variation of LRFS. The right panel shows the variation of the peak frequency across the pulse window; peak amplitude (top window), phase variations (middle window), profile (bottom window).

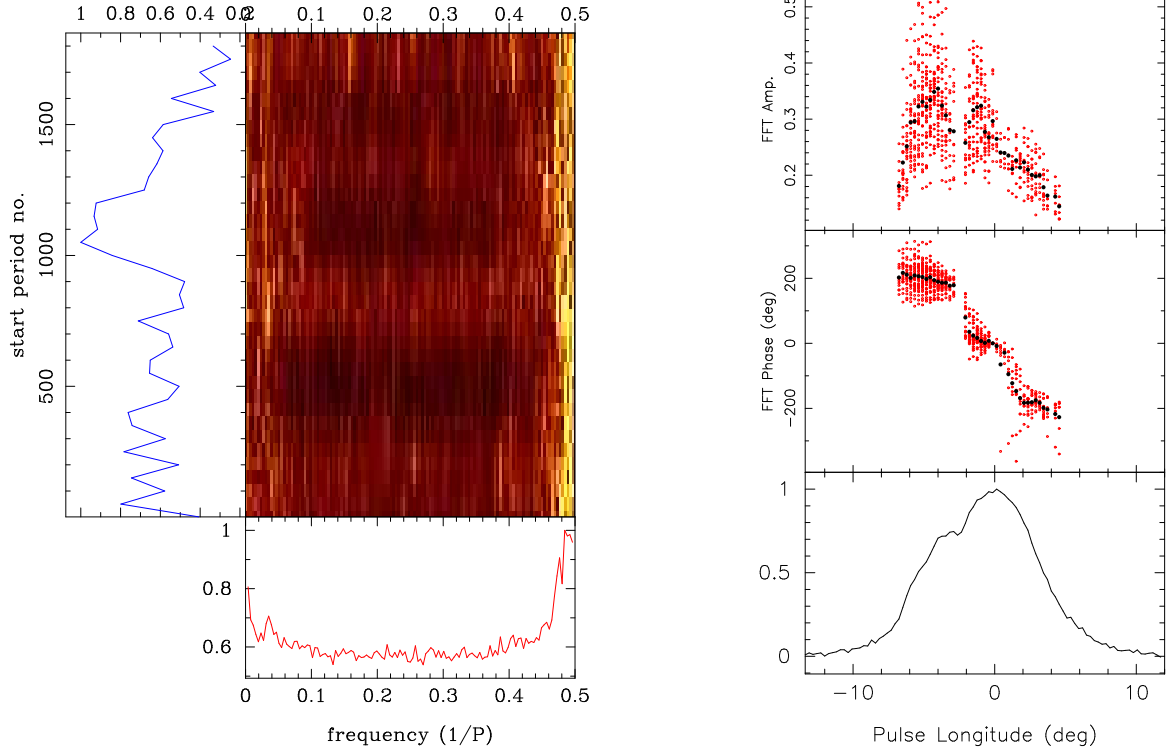


Figure A3. The fluctuation spectral analysis for PSR J0108+6608 at 339 MHz. The left panel shows time variation of LRFS. The right panel shows the variation of the peak frequency across the pulse window; peak amplitude (top window), phase variations (middle window), profile (bottom window).

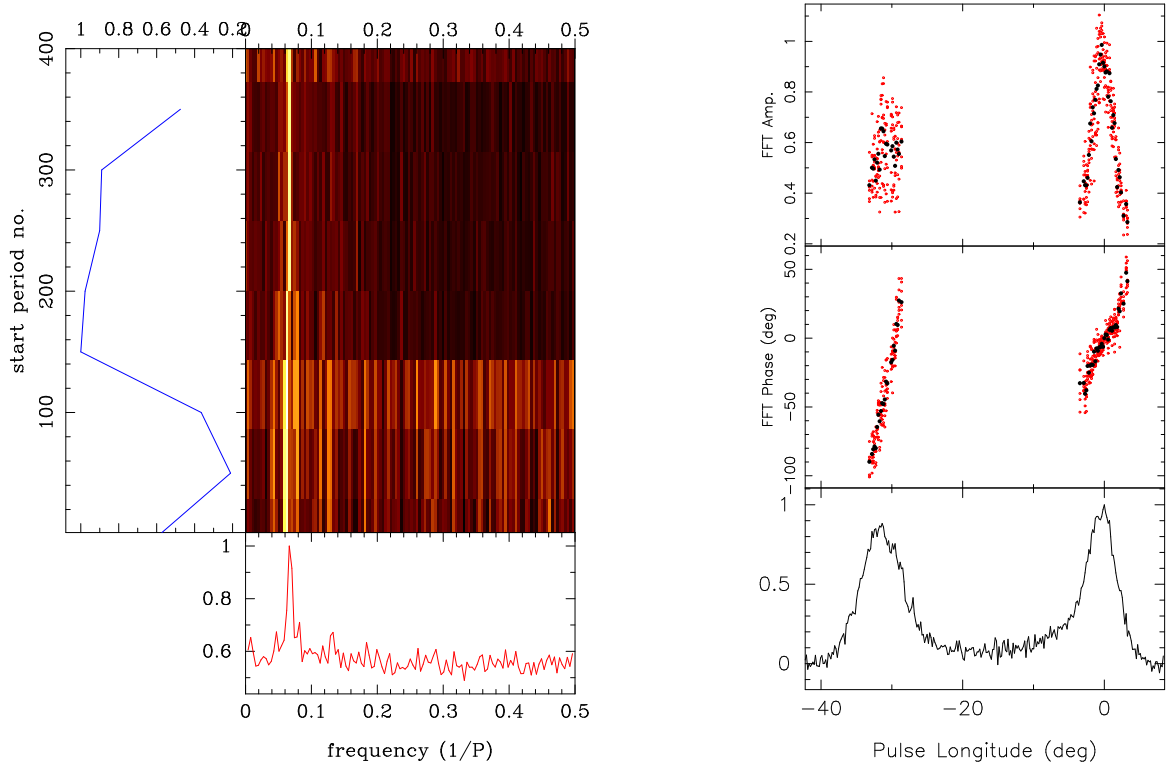


Figure A4. The fluctuation spectral analysis for PSR J0151-0635 at 333 MHz. The left panel shows time variation of LRFS. The right panel shows the variation of the peak frequency across the pulse window; peak amplitude (top window), phase variations (middle window), profile (bottom window).

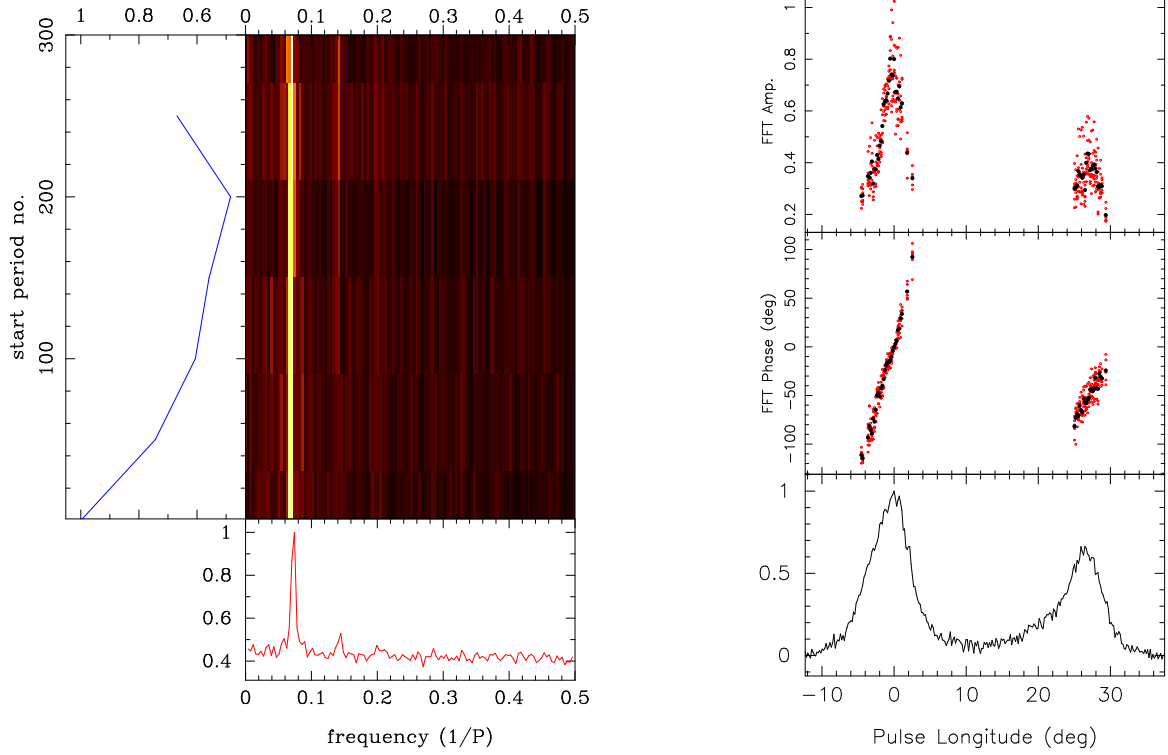


Figure A5. The fluctuation spectral analysis for PSR J0151–0635 at 618 MHz. The left panel shows time variation of LRFs. The right panel shows the variation of the peak frequency across the pulse window; peak amplitude (top window), phase variations (middle window), profile (bottom window).

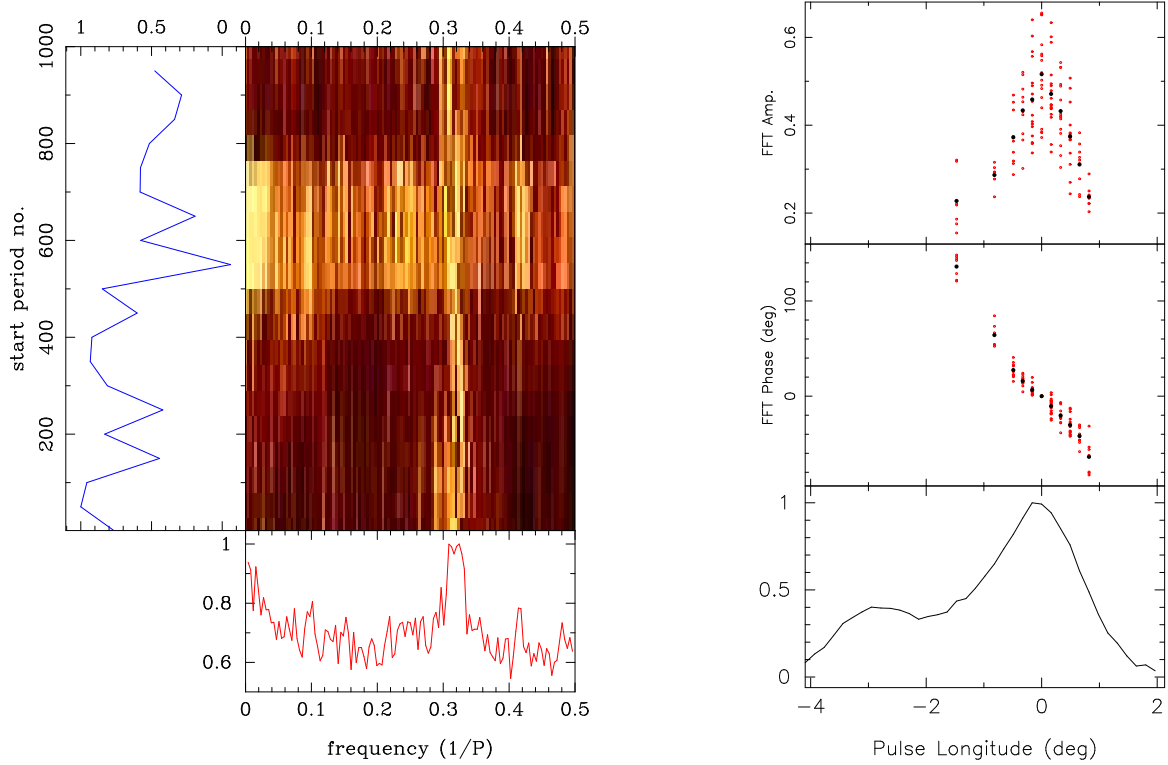


Figure A6. The fluctuation spectral analysis for PSR J0421–0345 at 339 MHz. The left panel shows time variation of LRFs. The right panel shows the variation of the peak frequency across the pulse window; peak amplitude (top window), phase variations (middle window), profile (bottom window).

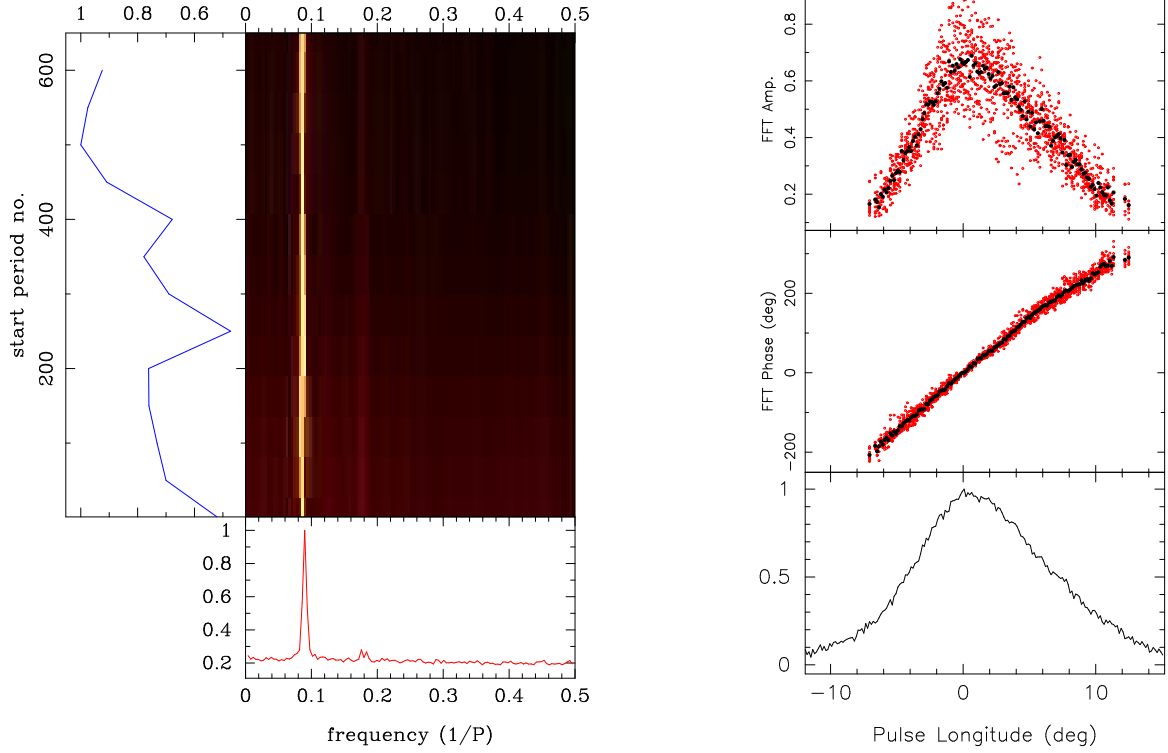


Figure A7. The fluctuation spectral analysis for PSR J0814+7429 at 325 MHz. The left panel shows time variation of LRFS. The right panel shows the variation of the peak frequency across the pulse window; peak amplitude (top window), phase variations (middle window), profile (bottom window).

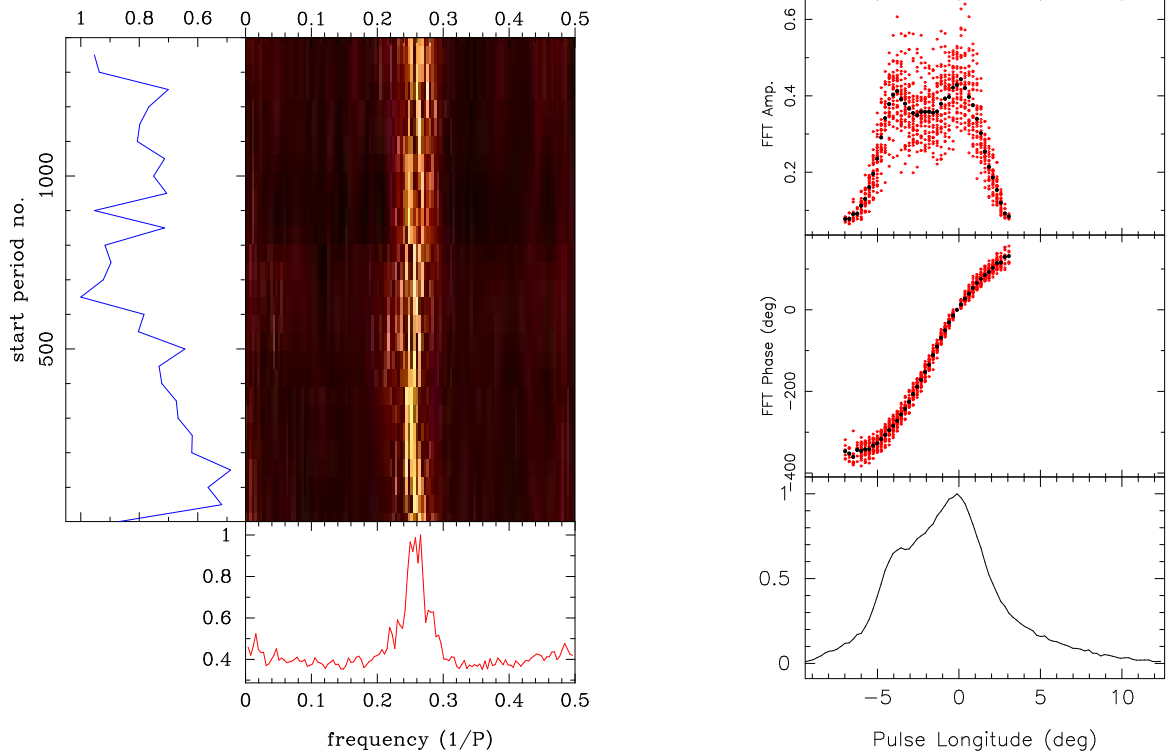


Figure A8. The fluctuation spectral analysis for PSR J0934-5249 at 339 MHz. The left panel shows time variation of LRFS. The right panel shows the variation of the peak frequency across the pulse window; peak amplitude (top window), phase variations (middle window), profile (bottom window).

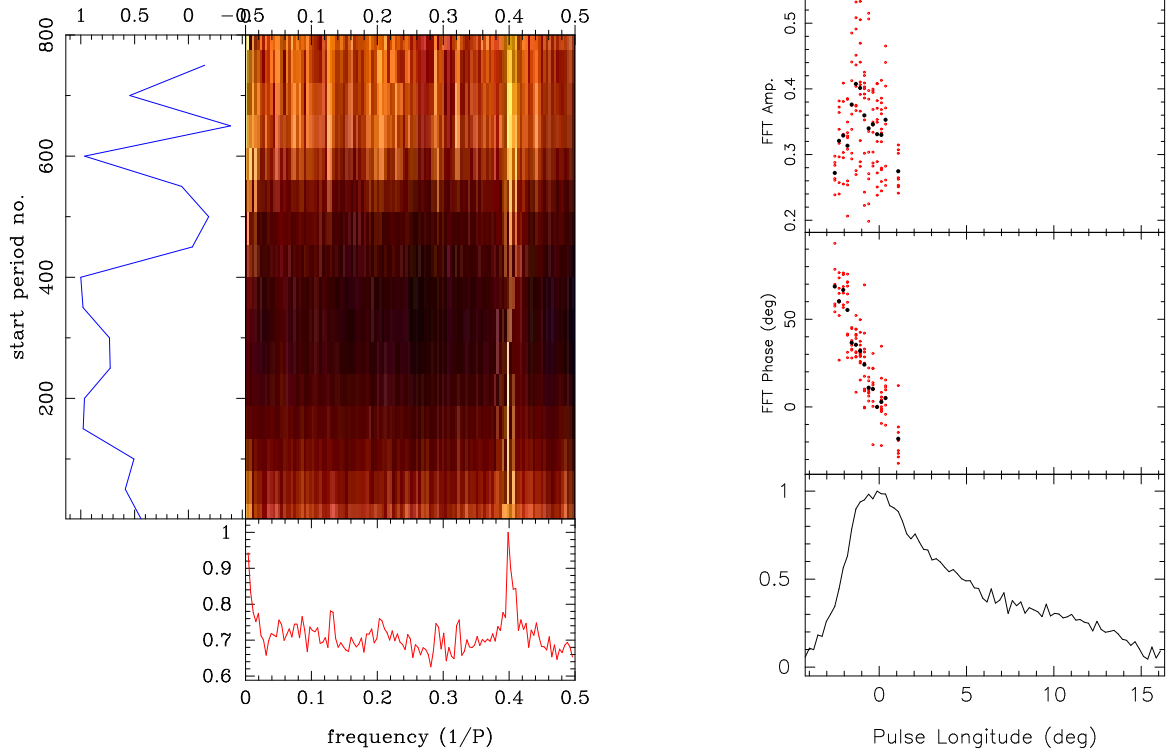


Figure A9. The fluctuation spectral analysis for PSR J1418–3921 at 618 MHz. The left panel shows time variation of LRFS. The right panel shows the variation of the peak frequency across the pulse window; peak amplitude (top window), phase variations (middle window), profile (bottom window).

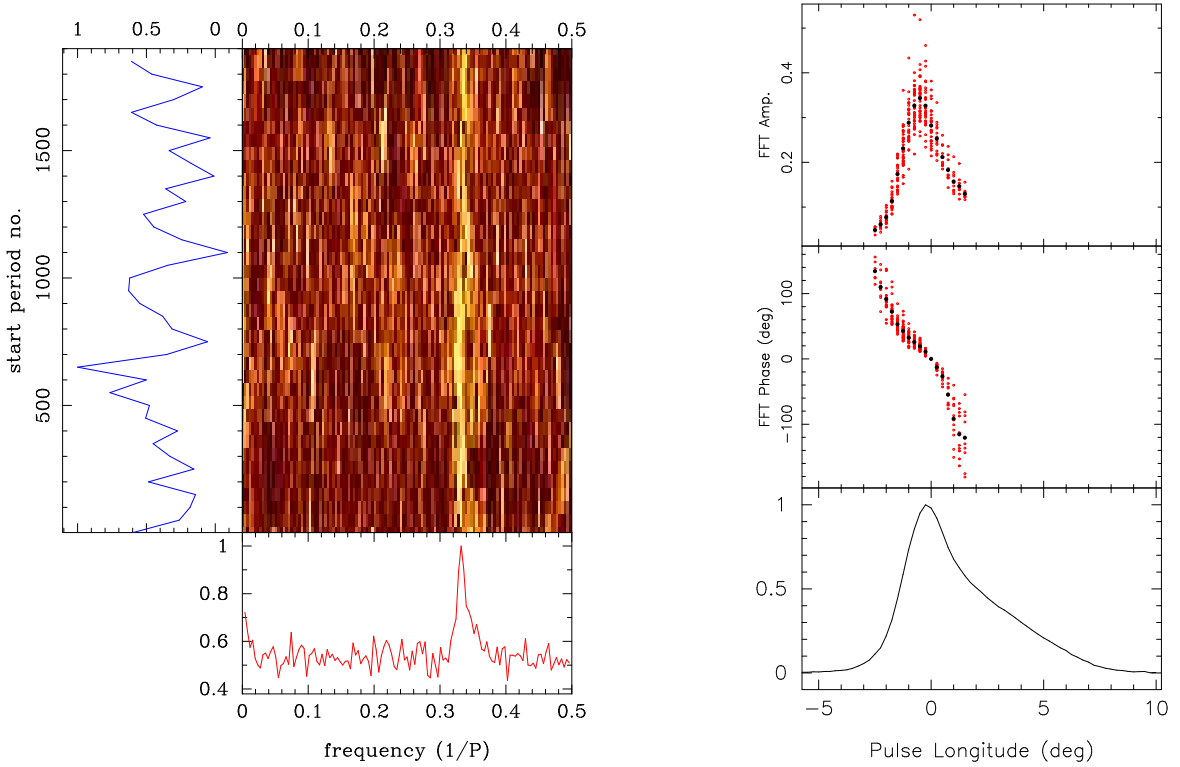


Figure A10. The fluctuation spectral analysis for PSR J1543–0620 at 339 MHz. The left panel shows time variation of LRFS. The right panel shows the variation of the peak frequency across the pulse window; peak amplitude (top window), phase variations (middle window), profile (bottom window).

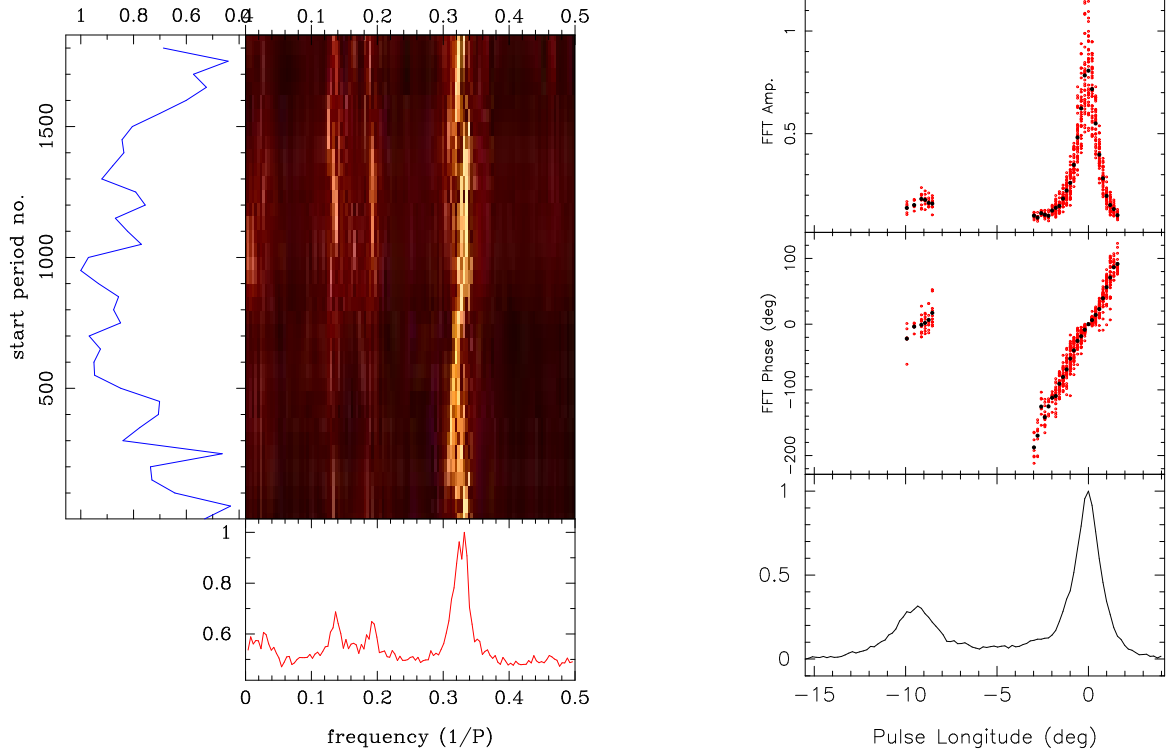


Figure A11. The fluctuation spectral analysis for PSR J1901–0906 at 333 MHz. The left panel shows time variation of LRFS. The right panel shows the variation of the peak frequency across the pulse window; peak amplitude (top window), phase variations (middle window), profile (bottom window).

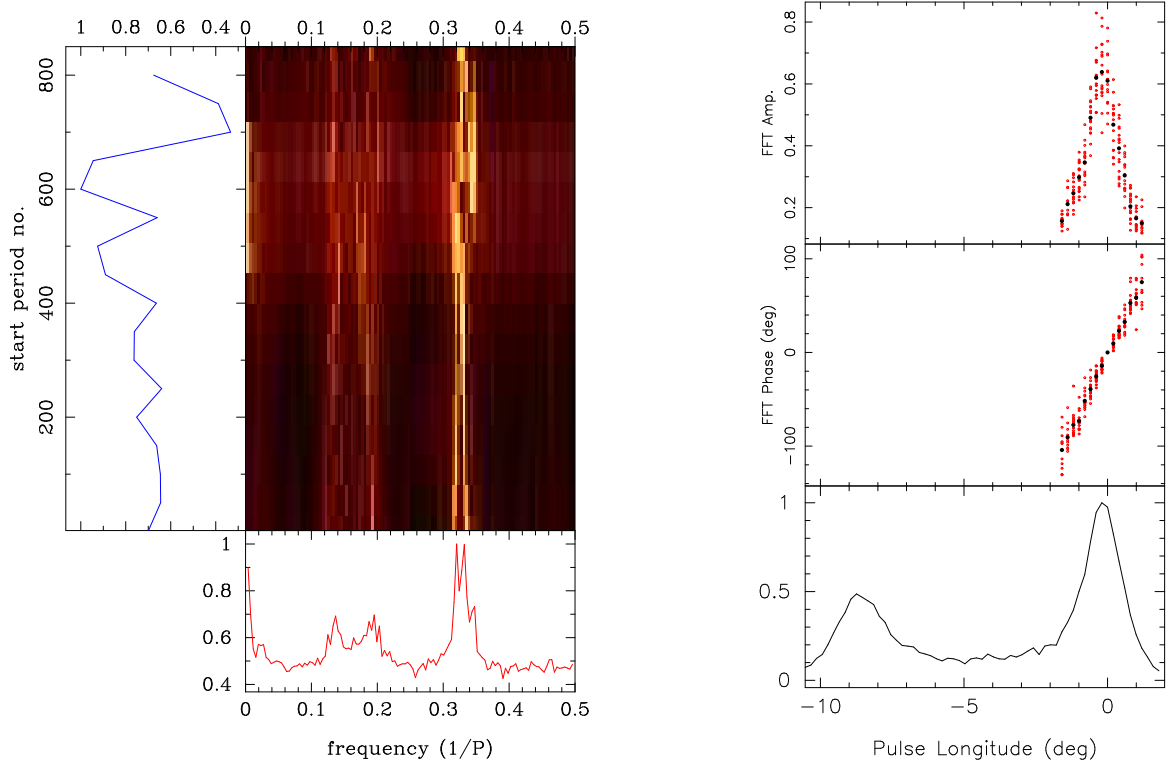


Figure A12. The fluctuation spectral analysis for PSR J1901–0906 at 618 MHz. The left panel shows time variation of LRFS. The right panel shows the variation of the peak frequency across the pulse window; peak amplitude (top window), phase variations (middle window), profile (bottom window).

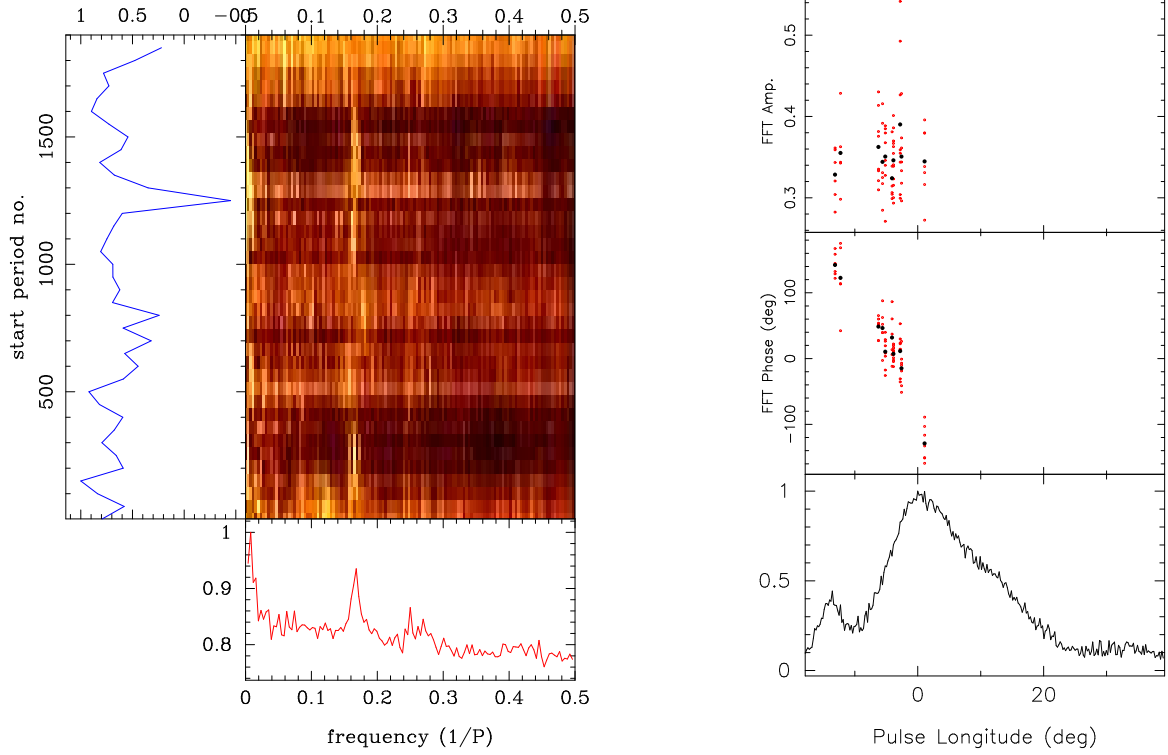


Figure A13. The fluctuation spectral analysis for PSR J1921+1948 at 333 MHz. The left panel shows time variation of LRFS. The right panel shows the variation of the peak frequency across the pulse window; peak amplitude (top window), phase variations (middle window), profile (bottom window).

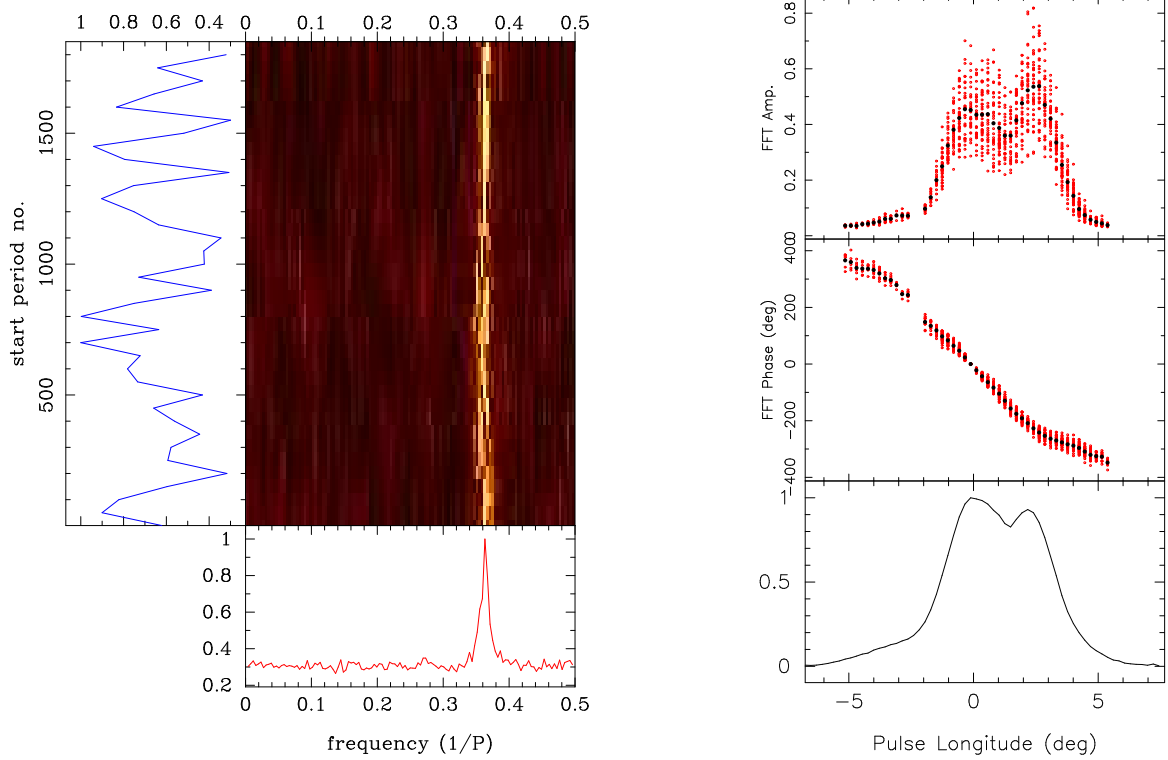


Figure A14. The fluctuation spectral analysis for PSR J2046-0421 at 333 MHz. The left panel shows time variation of LRFS. The right panel shows the variation of the peak frequency across the pulse window; peak amplitude (top window), phase variations (middle window), profile (bottom window).

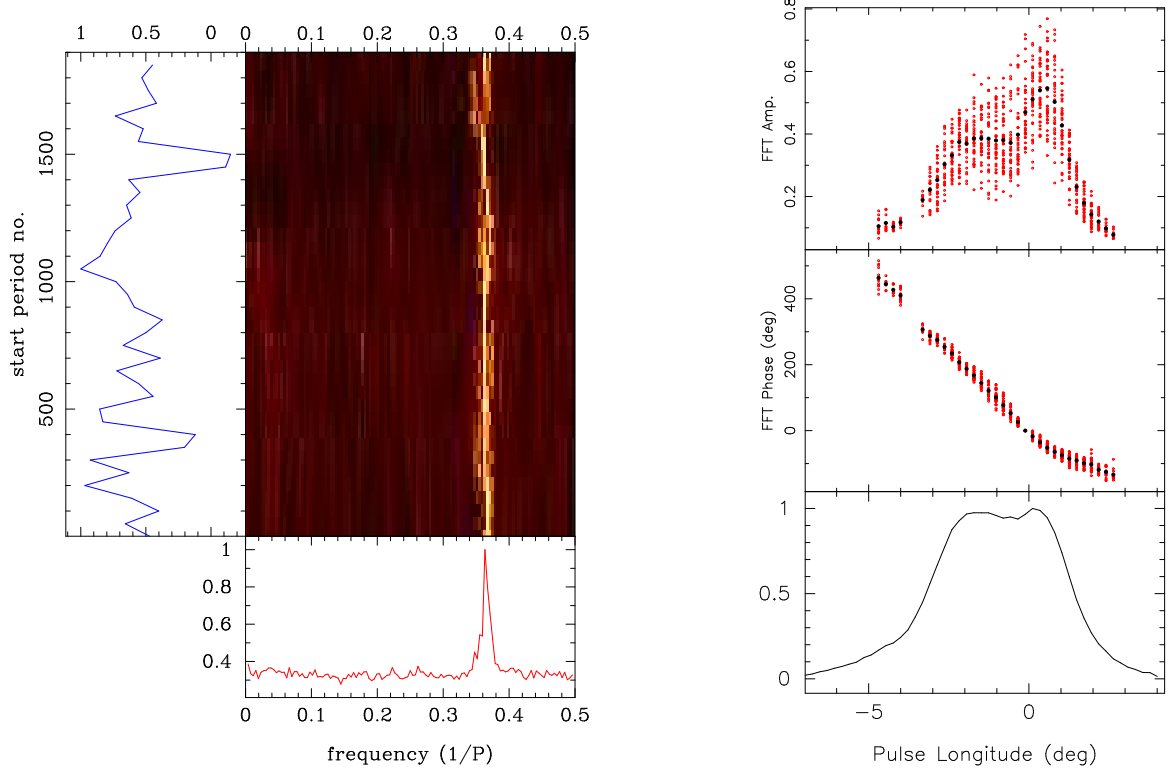


Figure A15. The fluctuation spectral analysis for PSR J2046–0421 at 618 MHz. The left panel shows time variation of LRFS. The right panel shows the variation of the peak frequency across the pulse window; peak amplitude (top window), phase variations (middle window), profile (bottom window).

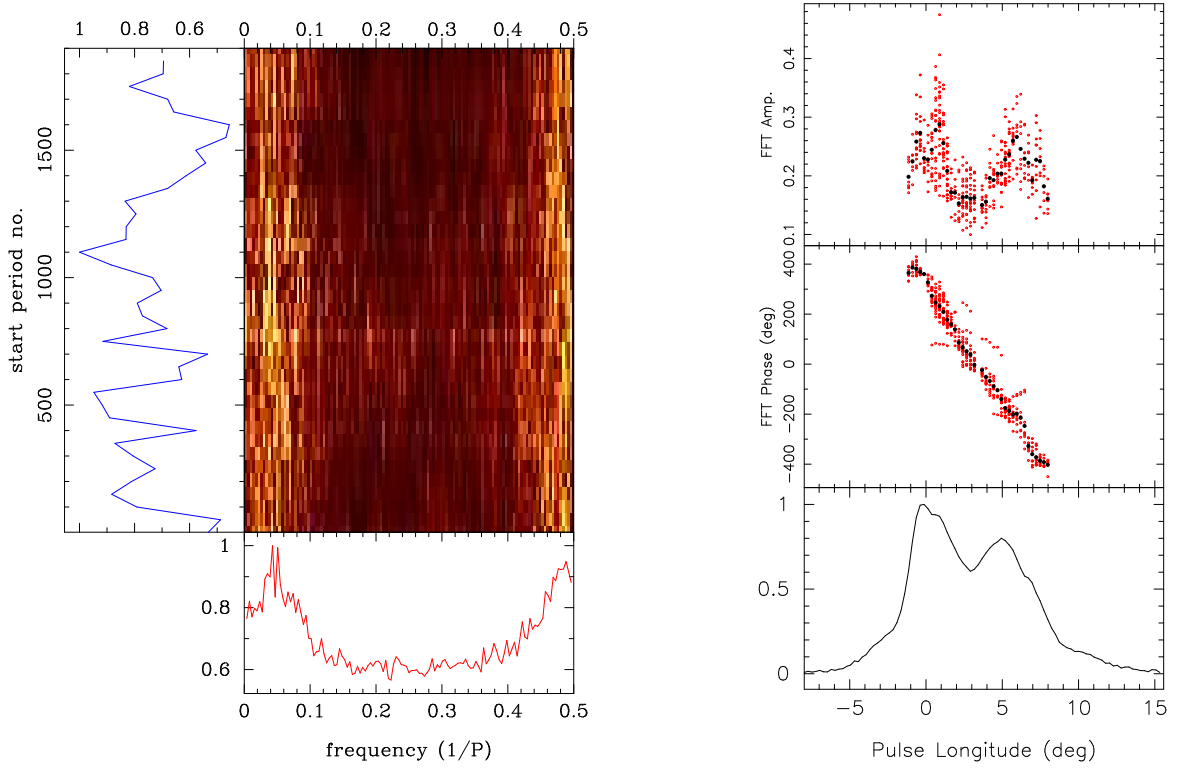


Figure A16. The fluctuation spectral analysis for PSR J2313+4253 at 339 MHz. The left panel shows time variation of LRFS. The right panel shows the variation of the peak frequency across the pulse window; peak amplitude (top window), phase variations (middle window), profile (bottom window).

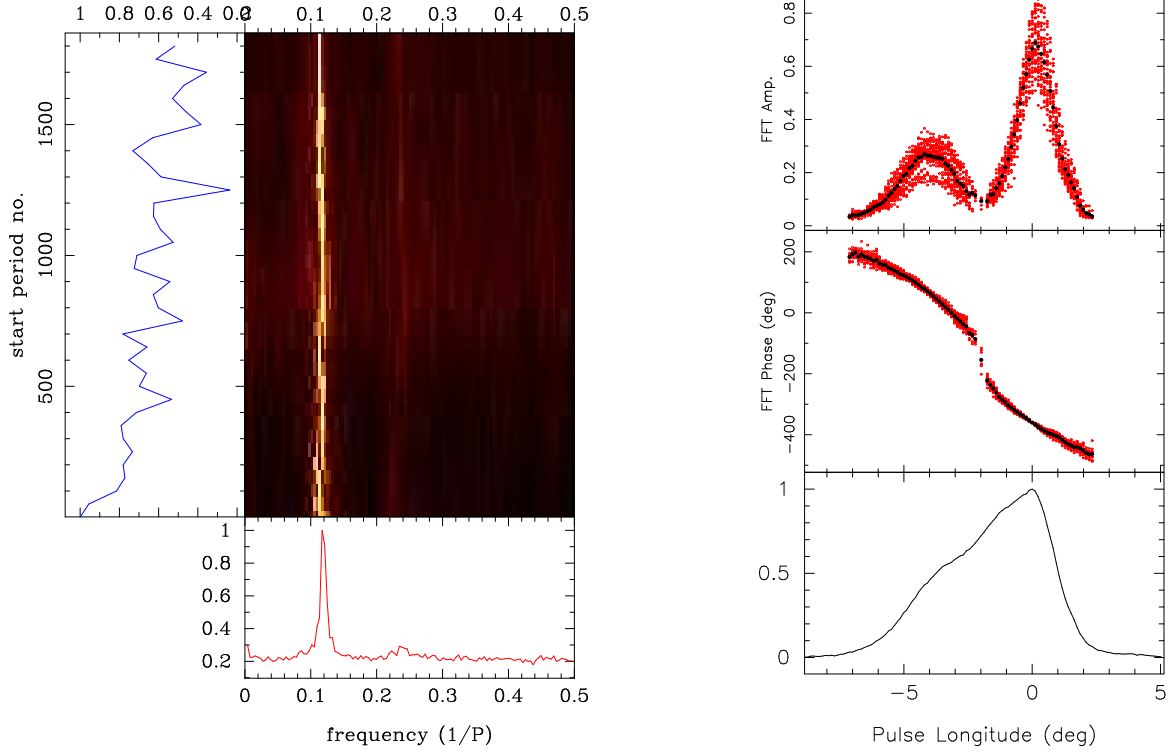


Figure B1. The fluctuation spectral analysis for PSR J0323+3944 at 339 MHz. The left panel shows time variation of LRFS. The right panel shows the variation of the peak frequency across the pulse window; peak amplitude (top window), phase variations (middle window), profile (bottom window).

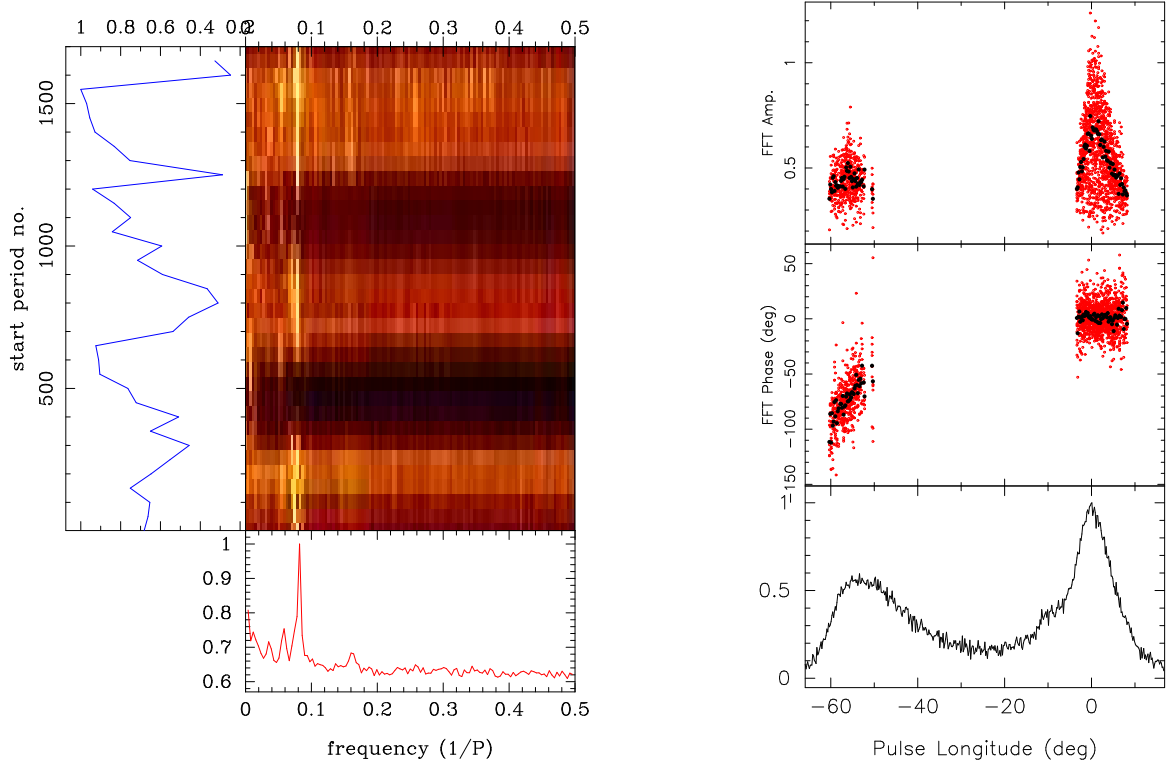


Figure B2. The fluctuation spectral analysis for PSR J1842-0359 at 618 MHz. The left panel shows time variation of LRFS. The right panel shows the variation of the peak frequency across the pulse window; peak amplitude (top window), phase variations (middle window), profile (bottom window).

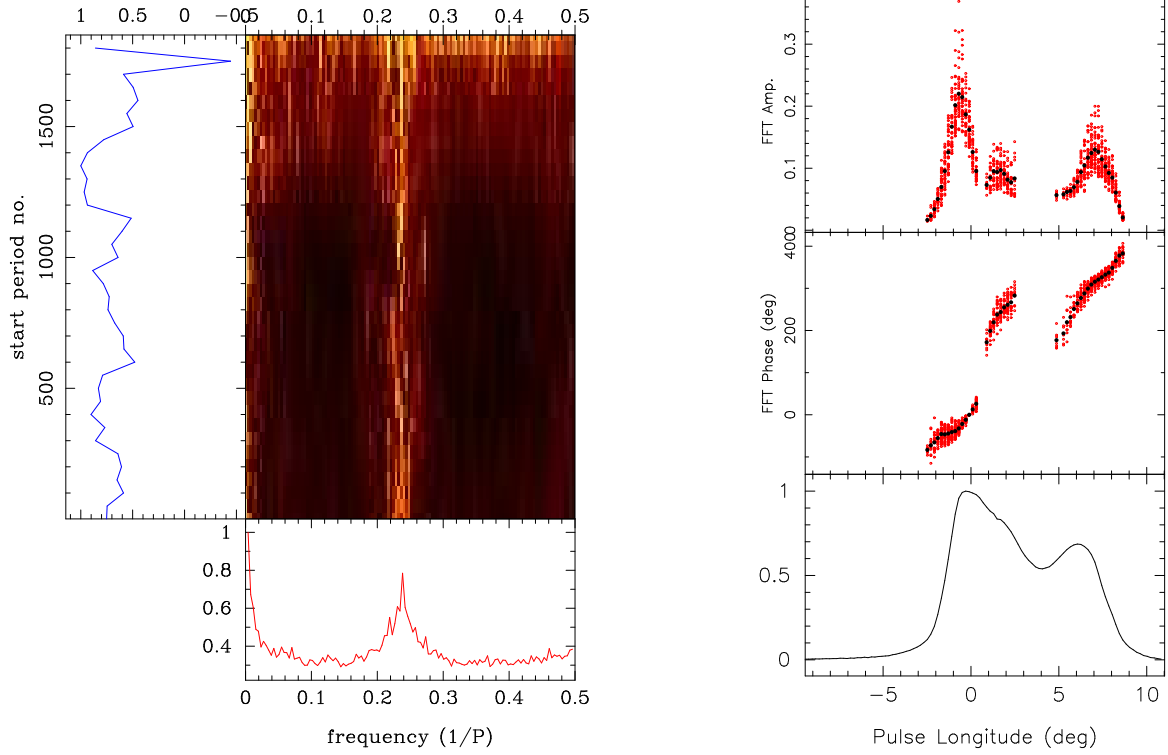


Figure B3. The fluctuation spectral analysis for PSR J1921+2153 at 618 MHz. The left panel shows time variation of LRFS. The right panel shows the variation of the peak frequency across the pulse window; peak amplitude (top window), phase variations (middle window), profile (bottom window).

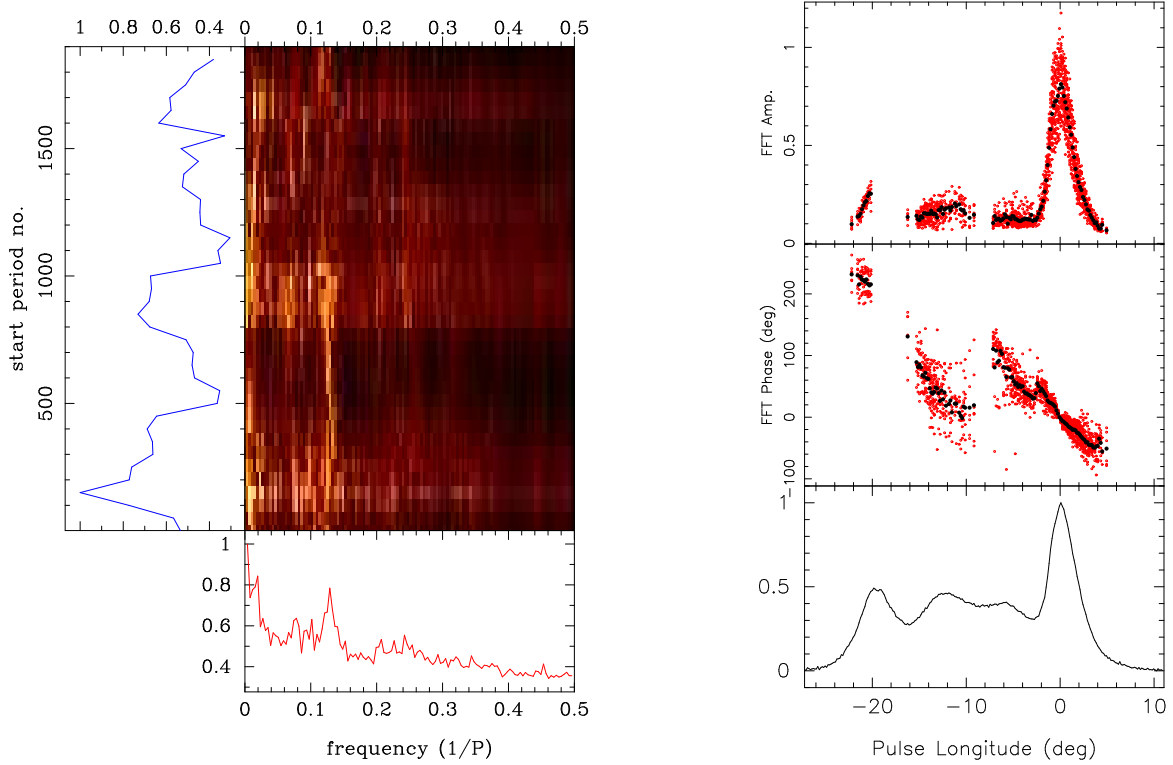


Figure B4. The fluctuation spectral analysis for PSR J2321+6024 at 339 MHz. The left panel shows time variation of LRFS. The right panel shows the variation of the peak frequency across the pulse window; peak amplitude (top window), phase variations (middle window), profile (bottom window). The peak frequency used in the right plot corresponds to $P_3 = 8P$.

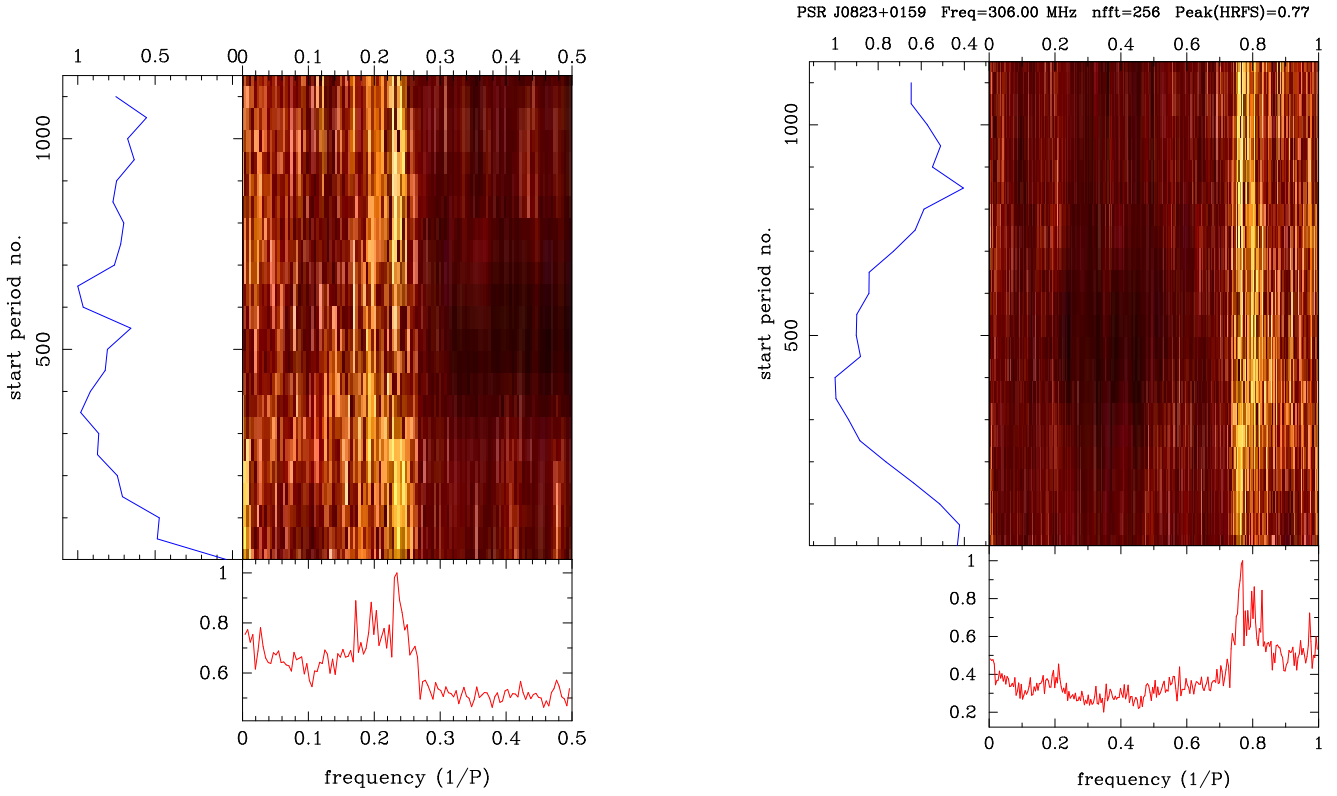


Figure C1. The fluctuation spectral analysis for PSR J0823+0159 at 339 MHz. The left panel shows time variation of LRFS. The right panel shows the time variation of HRFS.

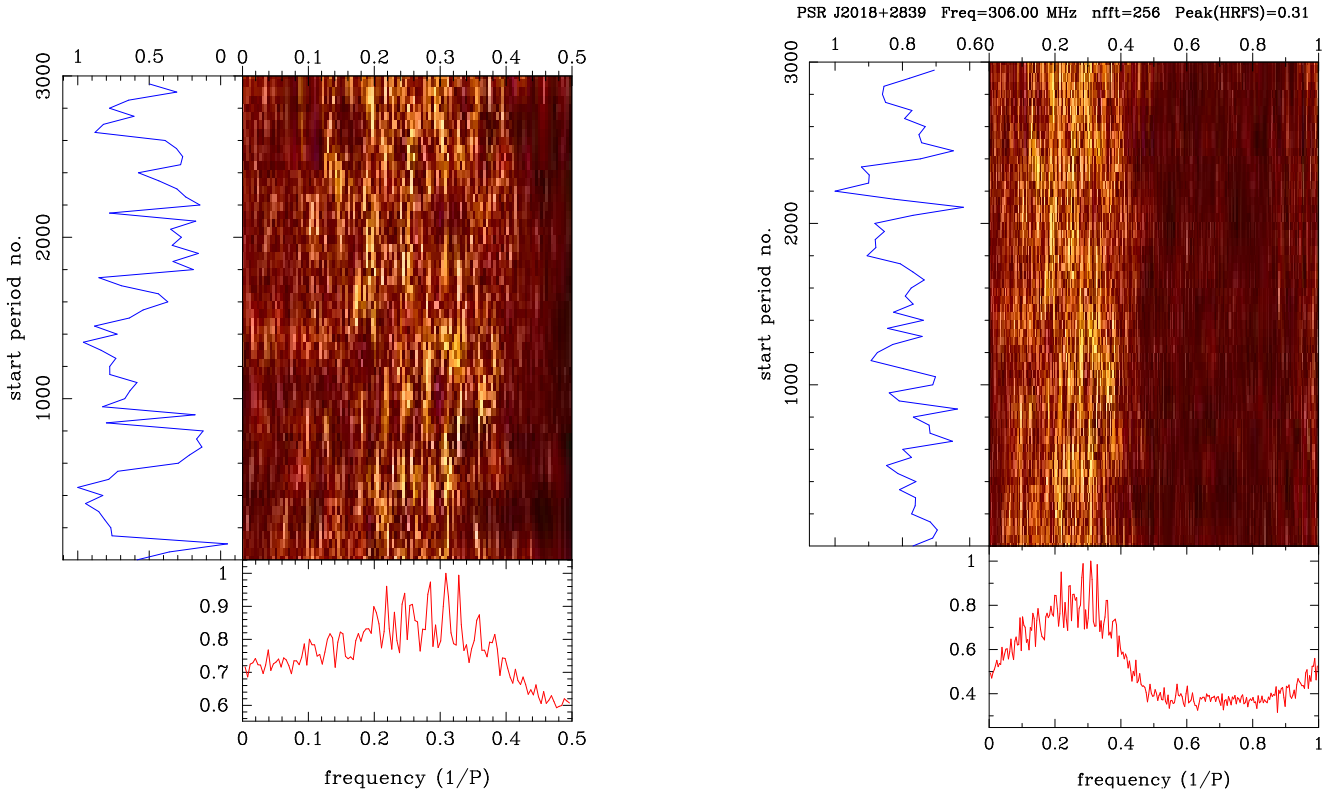


Figure C2. The fluctuation spectral analysis for PSR J2018+2839 at 339 MHz. The left panel shows time variation of LRFS. The right panel shows the time variation of HRFS.

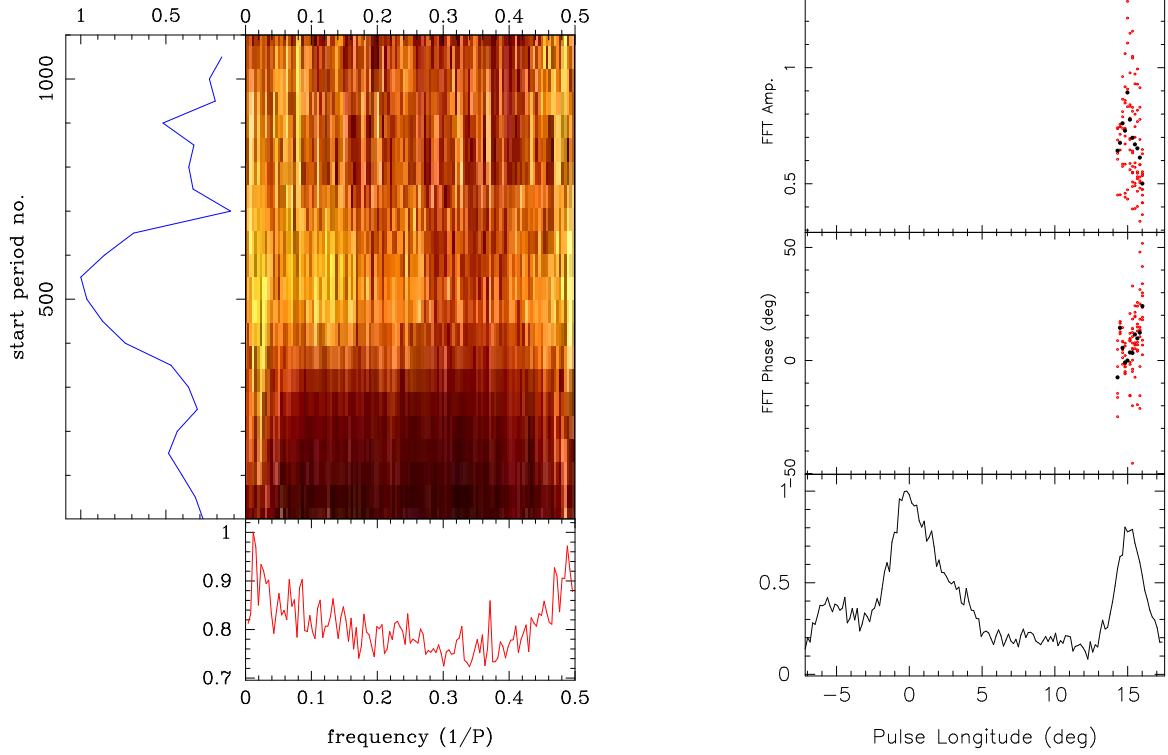


Figure D1. The fluctuation spectral analysis for PSR J0624–0424 at 339 MHz. The left panel shows time variation of LRFS. The right panel shows the variation of the peak frequency across the pulse window; peak amplitude (top window), phase variations (middle window), profile (bottom window).

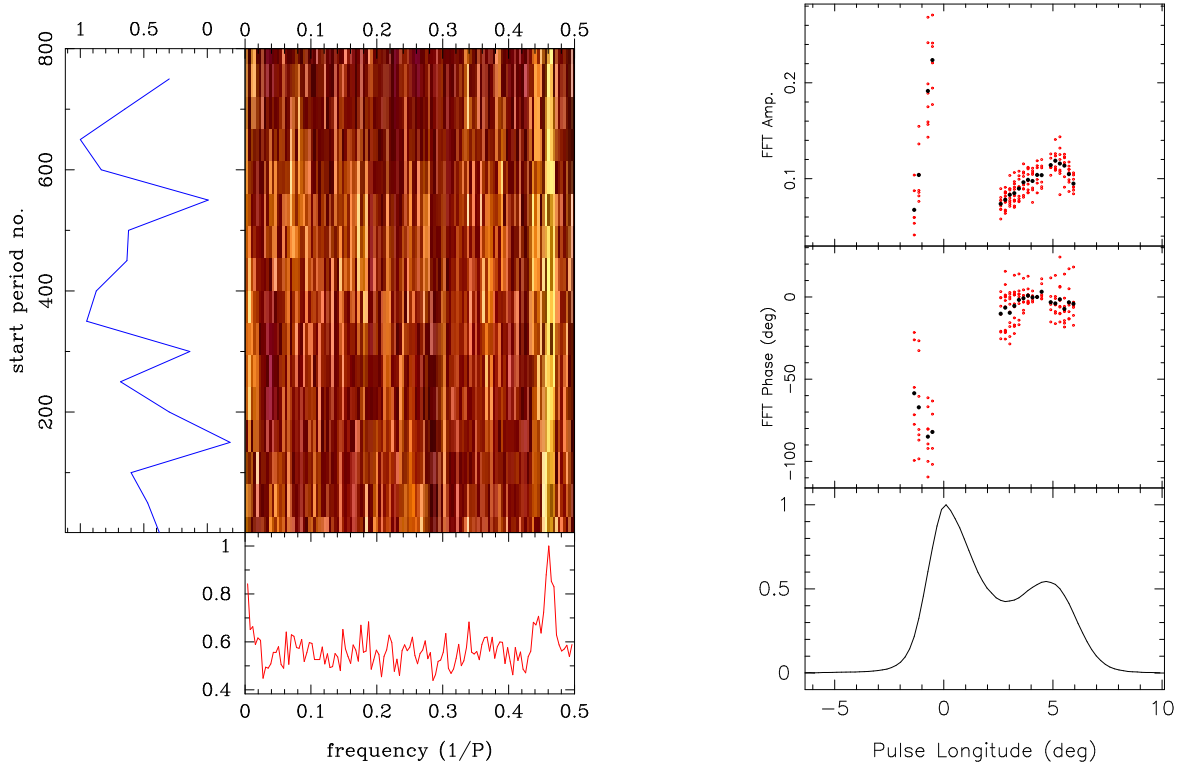


Figure D2. The fluctuation spectral analysis for PSR J0837+0610 at 333 MHz. The left panel shows time variation of LRFS. The right panel shows the variation of the peak frequency across the pulse window; peak amplitude (top window), phase variations (middle window), profile (bottom window).

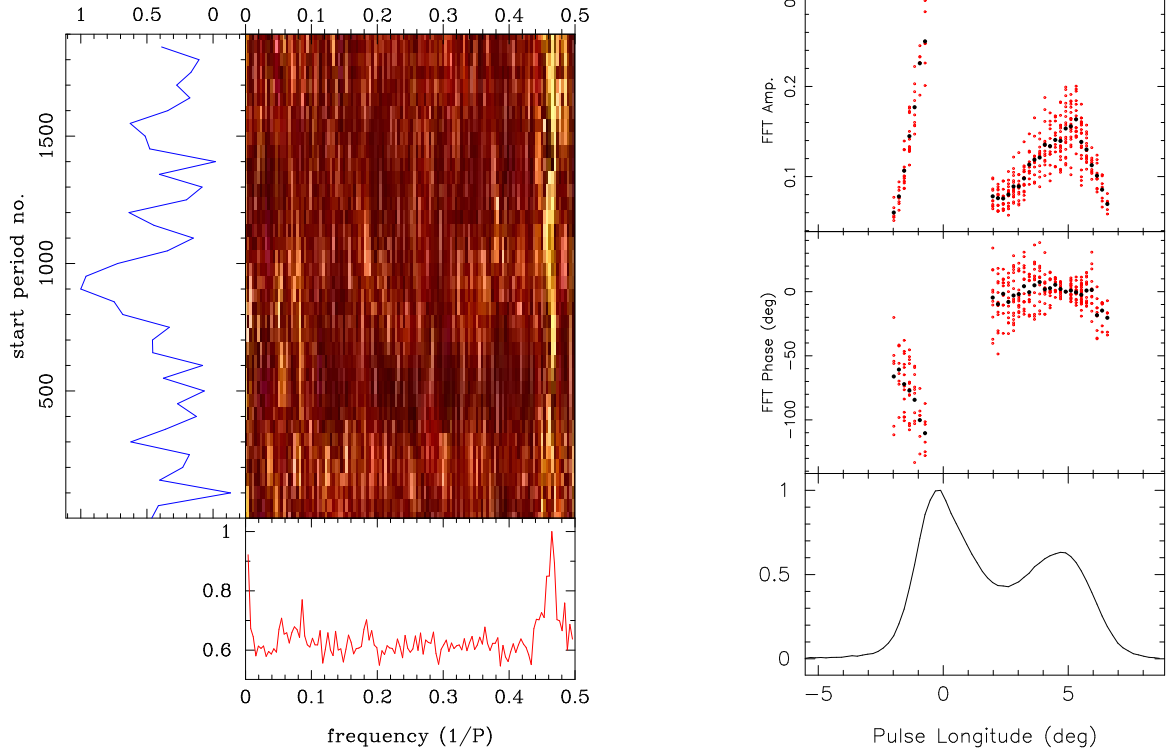


Figure D3. The fluctuation spectral analysis for PSR J0837+0610 at 618 MHz. The left panel shows time variation of LRFS. The right panel shows the variation of the peak frequency across the pulse window; peak amplitude (top window), phase variations (middle window), profile (bottom window).

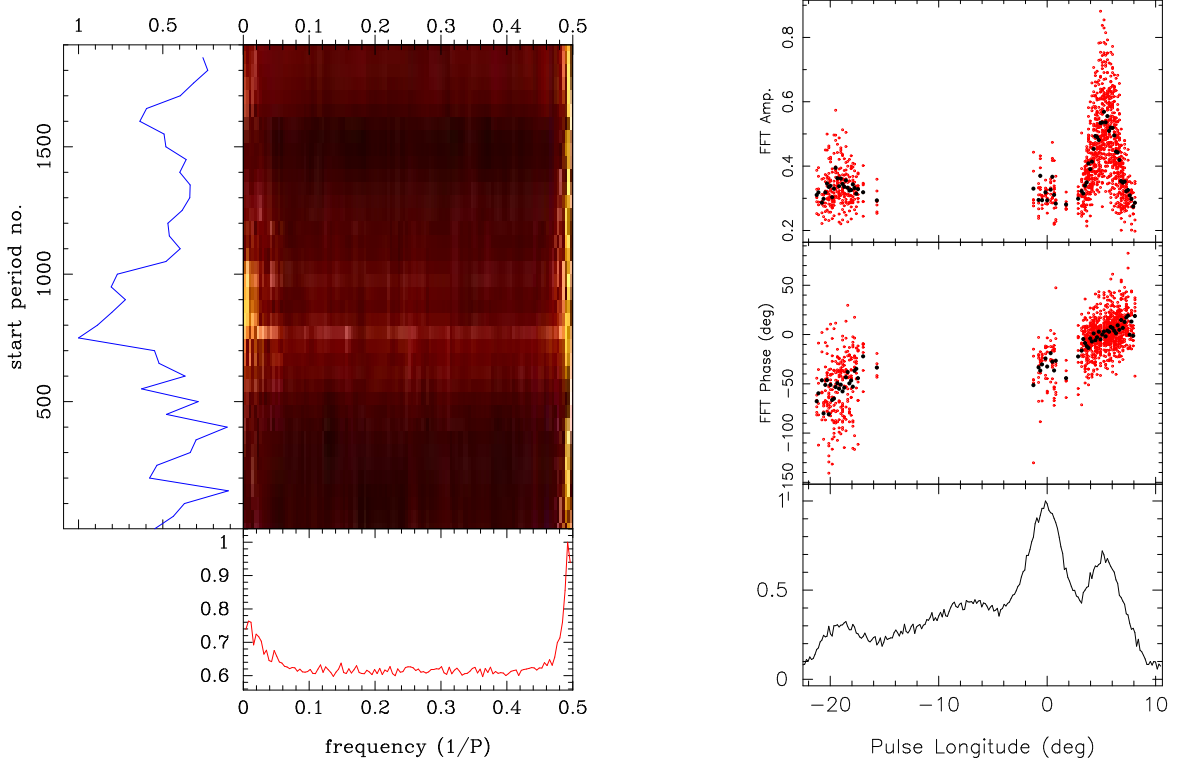


Figure D4. The fluctuation spectral analysis for PSR J0846-3533 at 333 MHz. The left panel shows time variation of LRFS. The right panel shows the variation of the peak frequency across the pulse window; peak amplitude (top window), phase variations (middle window), profile (bottom window).

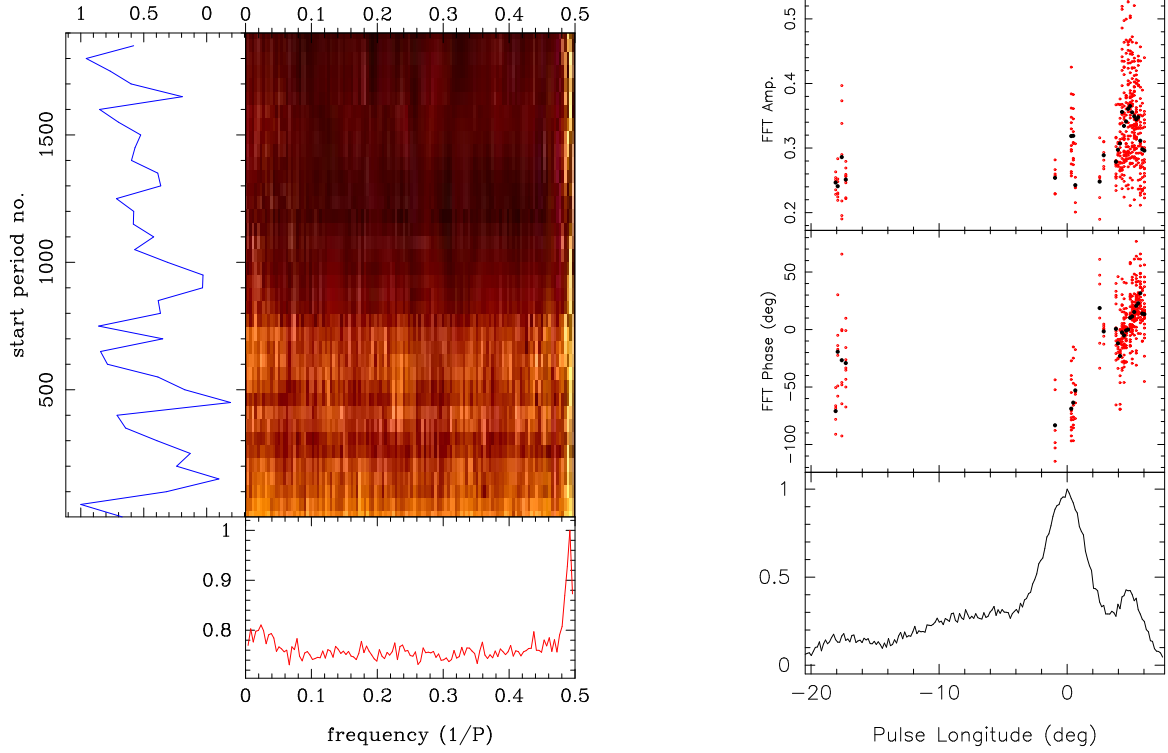


Figure D5. The fluctuation spectral analysis for PSR J0846–3533 at 618 MHz. The left panel shows time variation of LRFS. The right panel shows the variation of the peak frequency across the pulse window; peak amplitude (top window), phase variations (middle window), profile (bottom window).

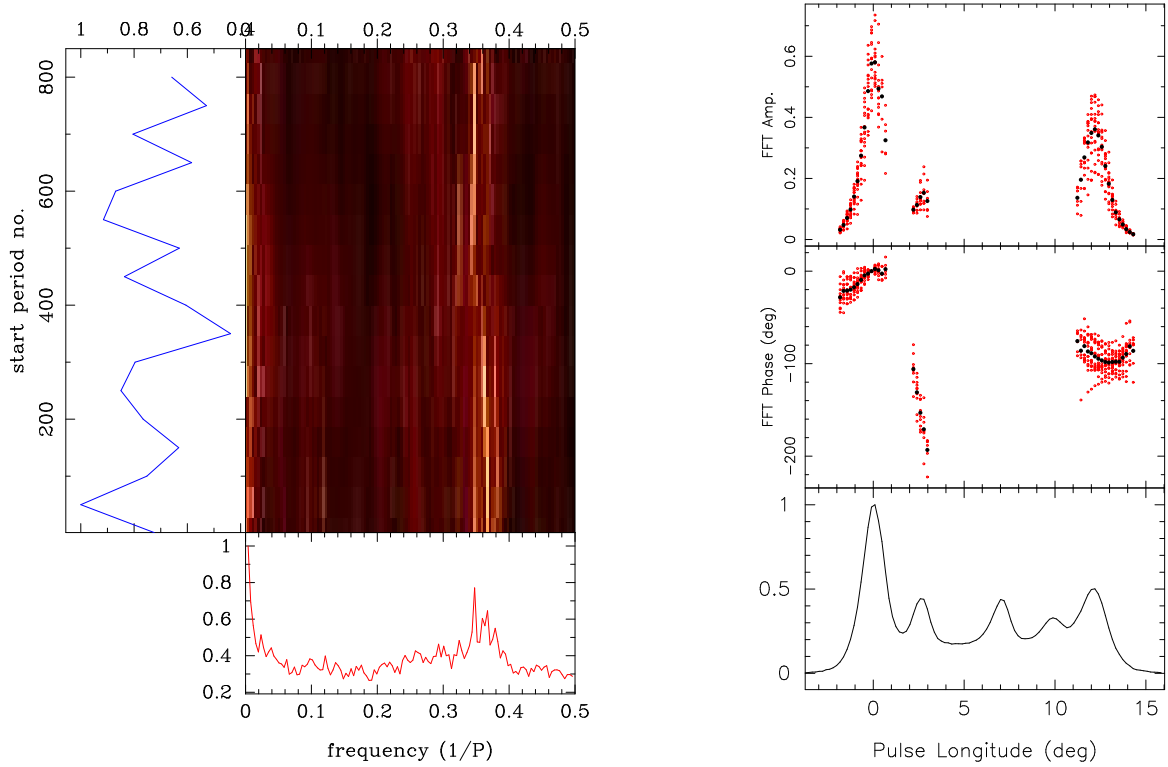


Figure D6. The fluctuation spectral analysis for PSR J1239+2453 at 333 MHz. The left panel shows time variation of LRFS. The right panel shows the variation of the peak frequency across the pulse window; peak amplitude (top window), phase variations (middle window), profile (bottom window).

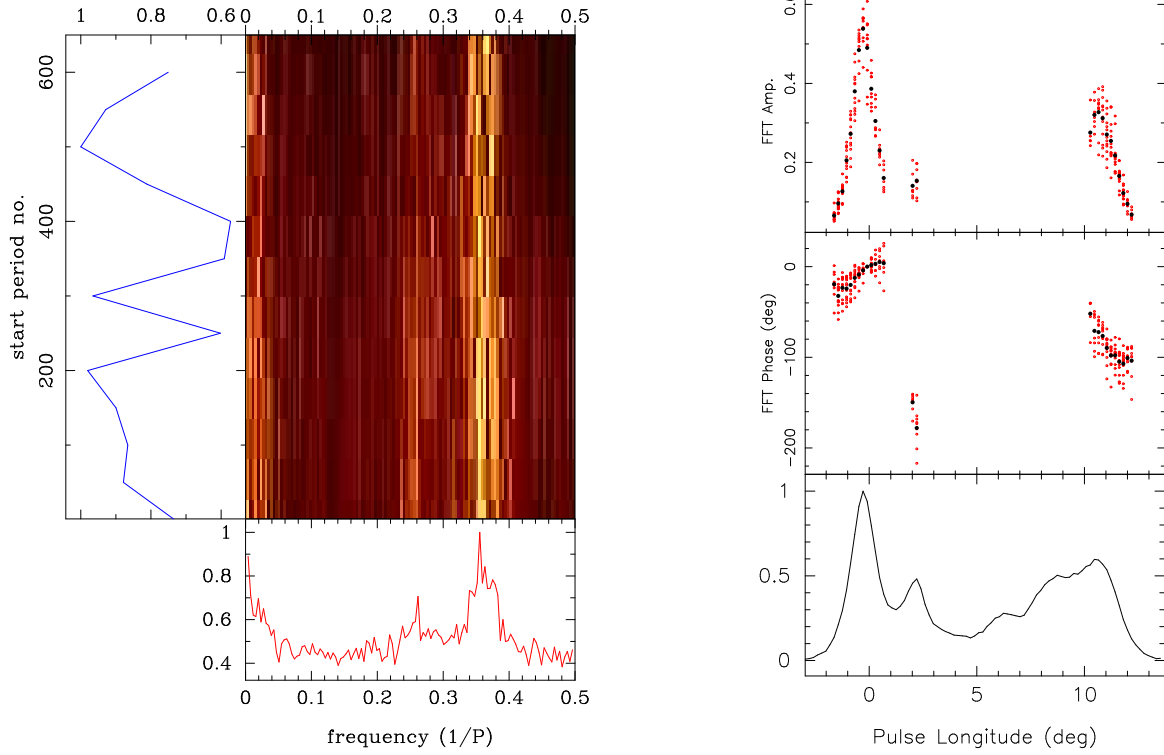


Figure D7. The fluctuation spectral analysis for PSR J1239+2453 at 618 MHz. The left panel shows time variation of LRFS. The right panel shows the variation of the peak frequency across the pulse window; peak amplitude (top window), phase variations (middle window), profile (bottom window).

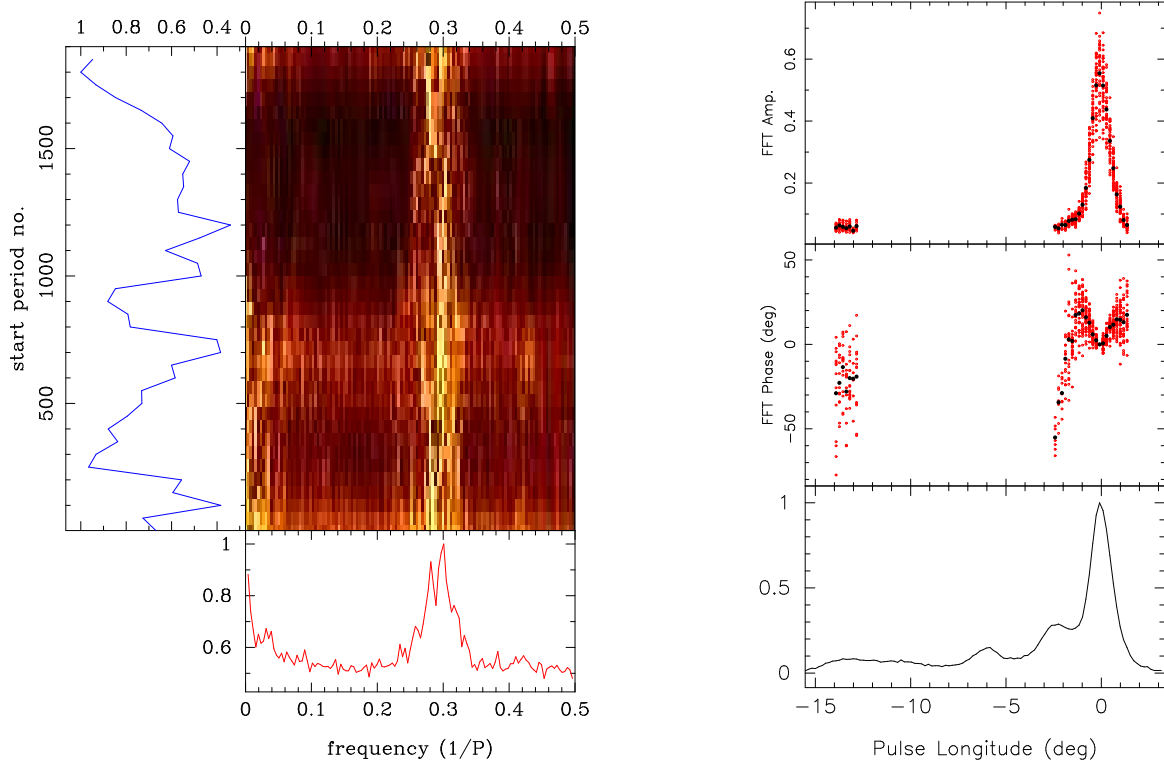


Figure D8. The fluctuation spectral analysis for PSR J1328-4921 at 333 MHz. The left panel shows time variation of LRFS. The right panel shows the variation of the peak frequency across the pulse window; peak amplitude (top window), phase variations (middle window), profile (bottom window).

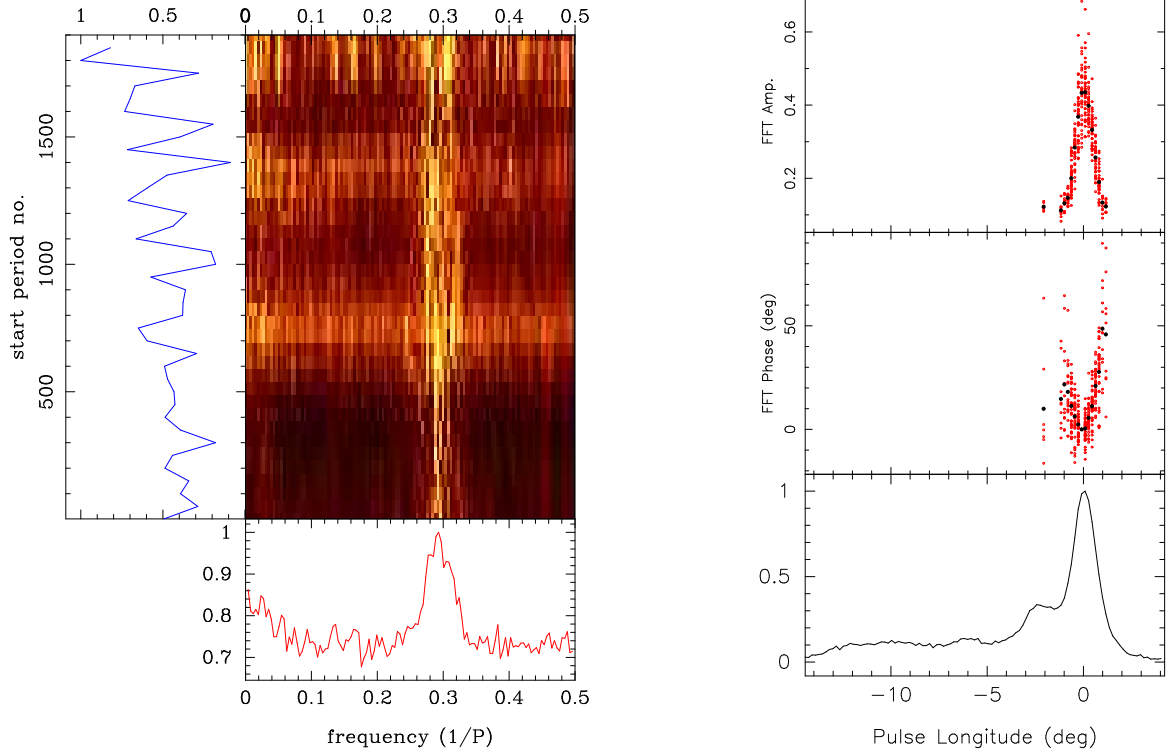


Figure D9. The fluctuation spectral analysis for PSR J1328–4921 at 618 MHz. The left panel shows time variation of LRFS. The right panel shows the variation of the peak frequency across the pulse window; peak amplitude (top window), phase variations (middle window), profile (bottom window).

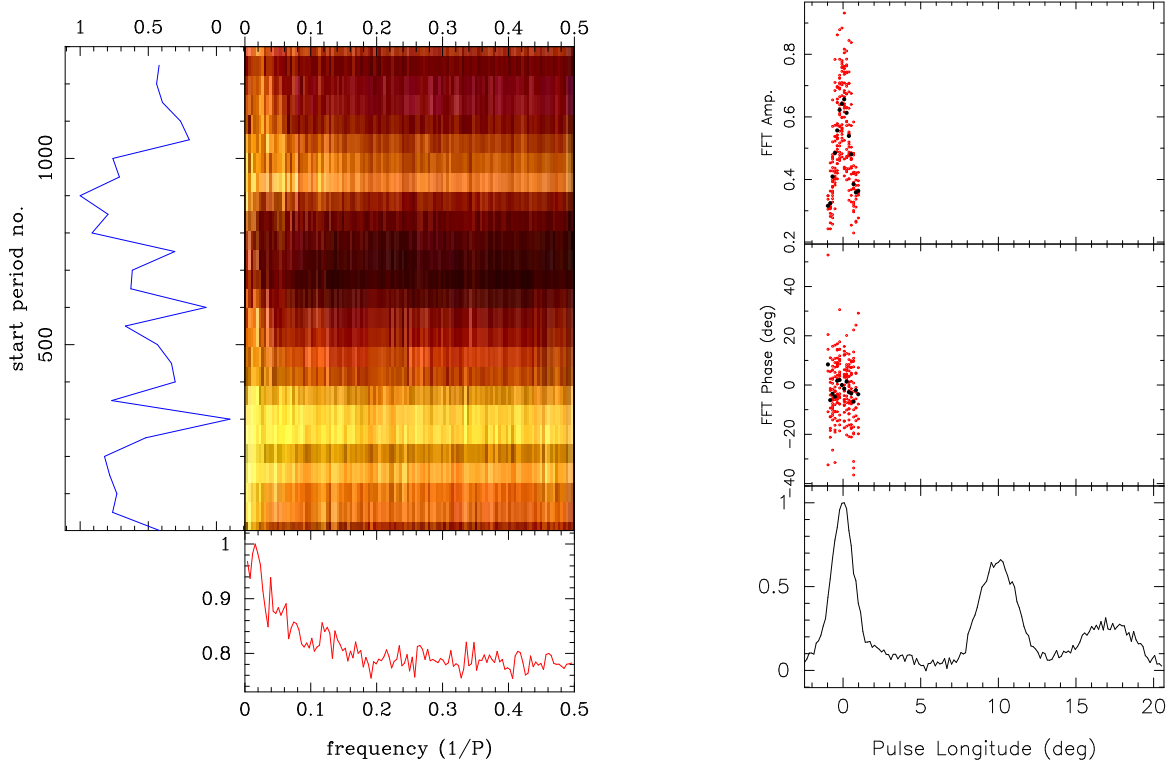


Figure D10. The fluctuation spectral analysis for PSR J1625–4048 at 618 MHz. The left panel shows time variation of LRFS. The right panel shows the variation of the peak frequency across the pulse window; peak amplitude (top window), phase variations (middle window), profile (bottom window).

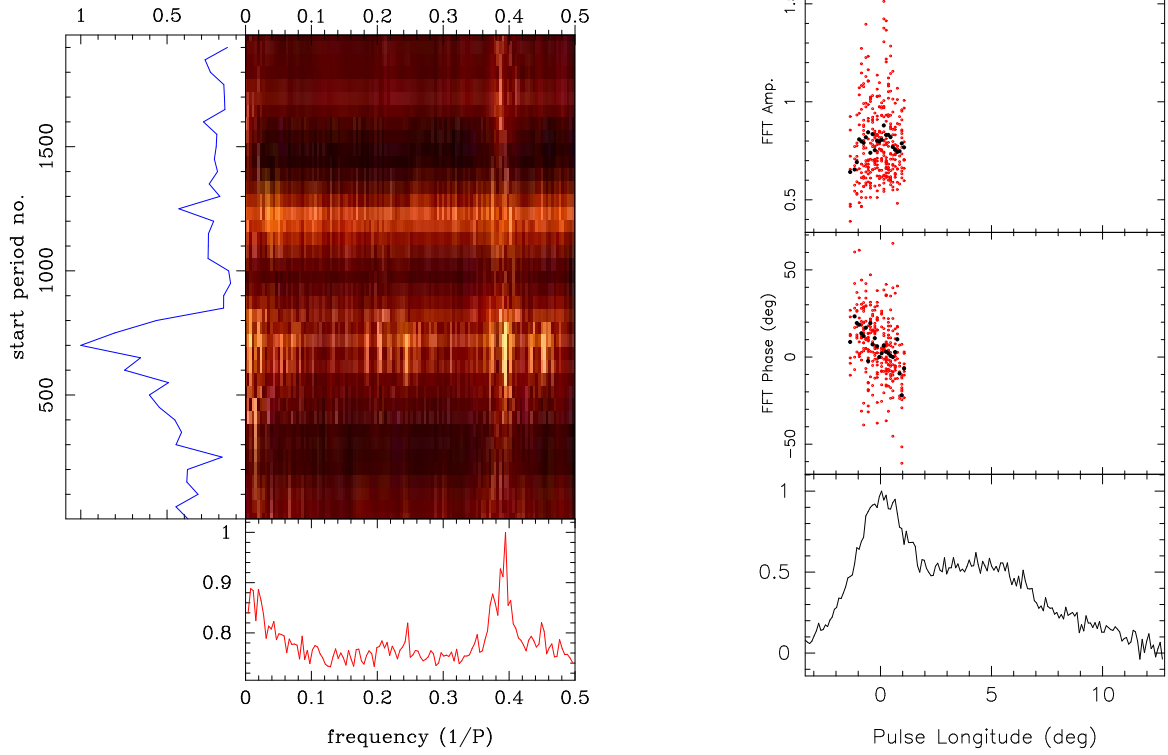


Figure D11. The fluctuation spectral analysis for PSR J1650–1654 at 339 MHz. The left panel shows time variation of LRFS. The right panel shows the variation of the peak frequency across the pulse window; peak amplitude (top window), phase variations (middle window), profile (bottom window).

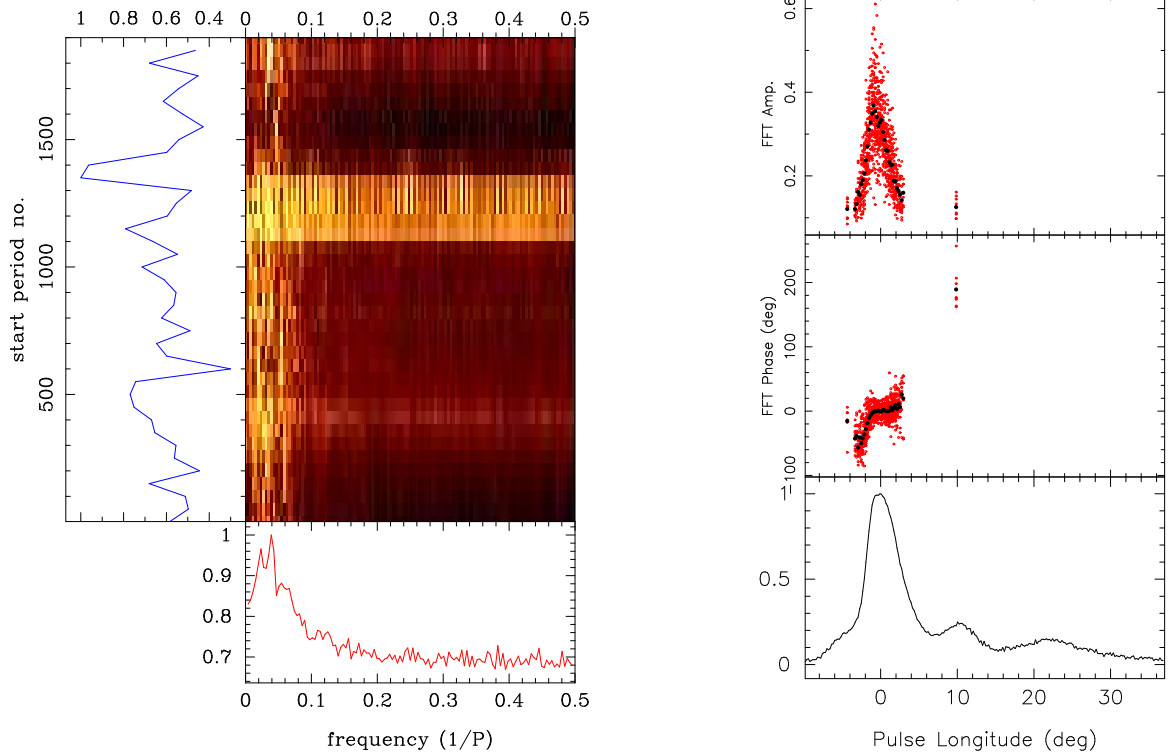


Figure D12. The fluctuation spectral analysis for PSR J1733–2228 at 333 MHz. The left panel shows time variation of LRFS. The right panel shows the variation of the peak frequency across the pulse window; peak amplitude (top window), phase variations (middle window), profile (bottom window).

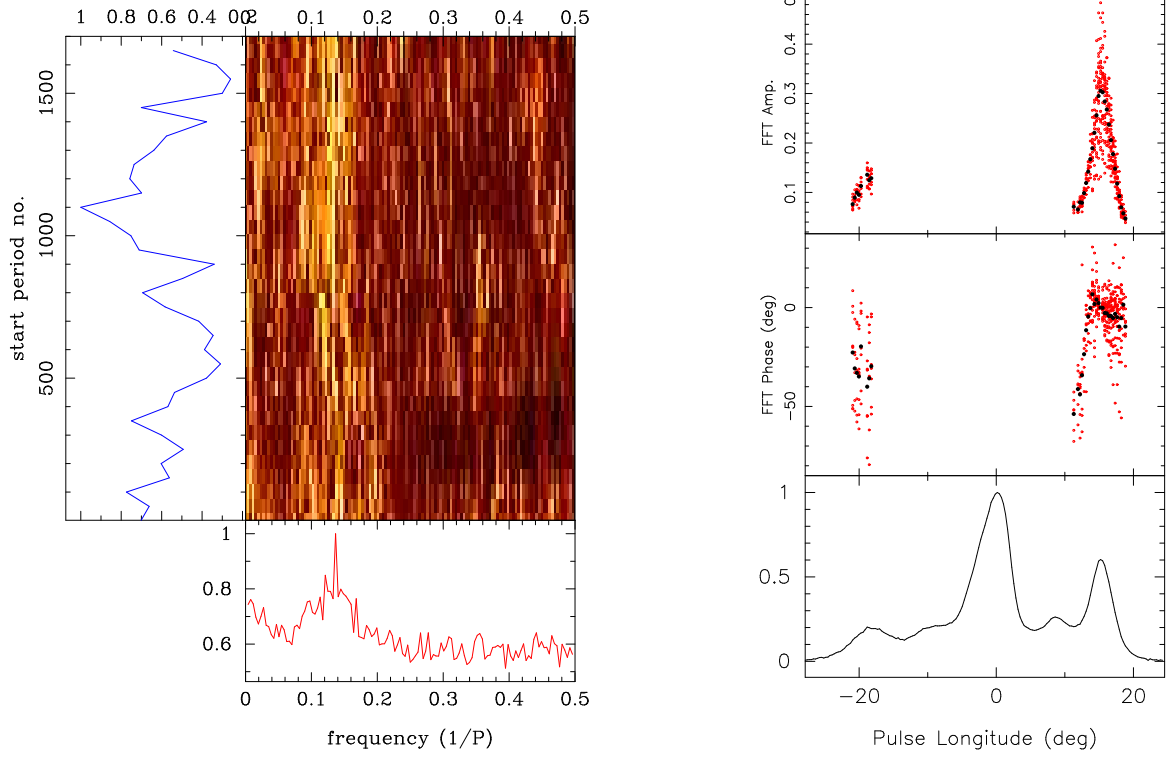


Figure D13. The fluctuation spectral analysis for PSR J1900–2600 at 325 MHz. The left panel shows time variation of LRFS. The right panel shows the variation of the peak frequency across the pulse window; peak amplitude (top window), phase variations (middle window), profile (bottom window).

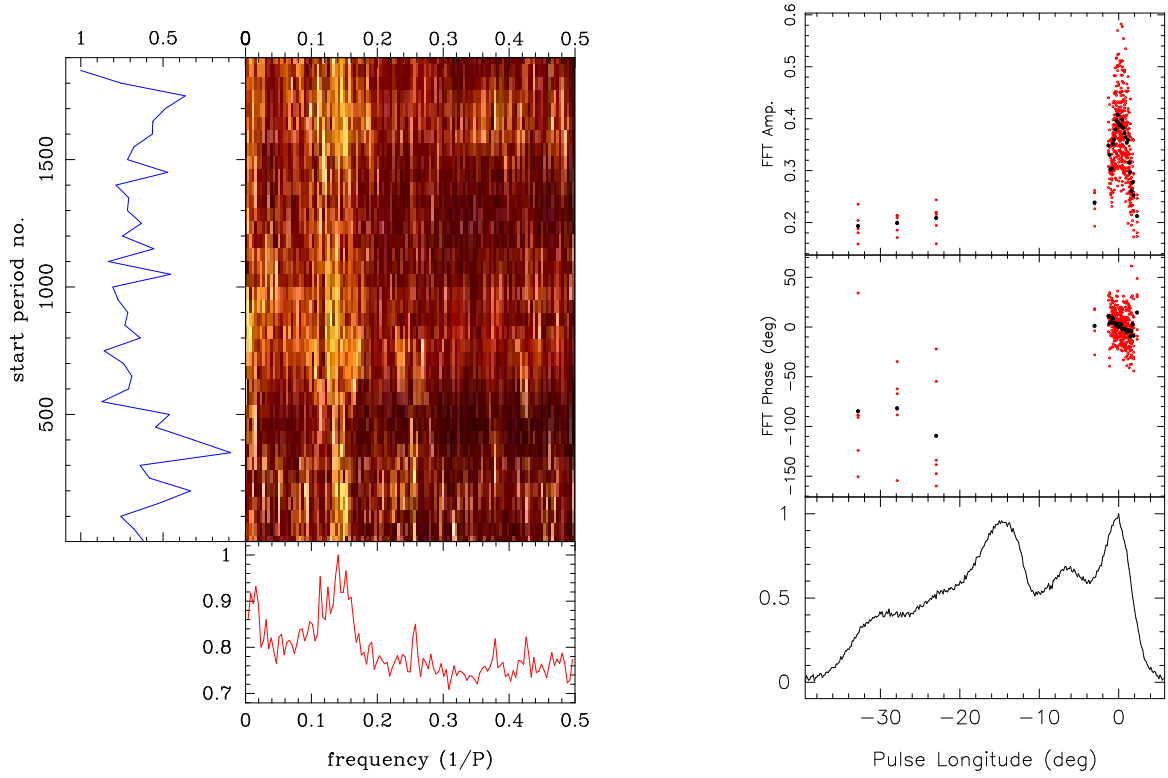


Figure D14. The fluctuation spectral analysis for PSR J1900–2600 at 618 MHz. The left panel shows time variation of LRFS. The right panel shows the variation of the peak frequency across the pulse window; peak amplitude (top window), phase variations (middle window), profile (bottom window).